

1

**SECOND SEMI-ANNUAL TECHNICAL REPORT**

**ELECTRICAL and OPTICAL PROPERTIES of AMORPHOUS MATERIALS\***

by

A Solid-State Group of the Physics Department  
Northern Illinois University  
DeKalb, Illinois 60115

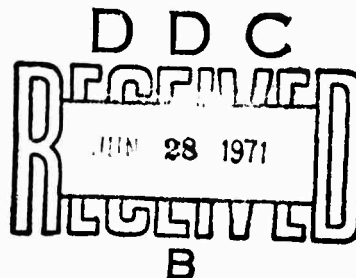
\*Sponsored by  
Advanced Research Projects Agency  
ARPA Order No. 1562

The views and conclusions contained in this document are those of the authors and should not be interpreted as necessarily representing the official policies, either expressed or implied, of the Advanced Research Projects Agency or the U. S. Government.

Reproduced by  
**NATIONAL TECHNICAL  
INFORMATION SERVICE**  
Springfield, Va. 22151

**DISTRIBUTION STATEMENT A**

Approved for public release;  
Distribution Unlimited



GENERAL INFORMATION

ARPA Order Number	1562
Program Code Number	0010
Name of Contractor	U. S. Army Research Office
Effective Date of Contract	June 1, 1970
Contract Expiration Date	May 31, 1971
Amount of Contract	\$45,868.00
Contract Number	DA-ARO-D-31-124-70-G77
Principal Investigator Phone Number	Dr. Charles Wood (815) 753-1773

## CONTENTS

### THEORETICAL RESEARCH

- I. The Kramers-Kronig (Hilbert) Transform 1
- II. Electronic Structure 2

### MATERIALS RESEARCH

- I. Amorphous Thin Films 4
- II. Crystalline Thin Films 4
- III. Single Crystals 5
- IV. Differential Thermal Analysis 5

### STRUCTURAL INVESTIGATIONS

- I. Mossbauer Studies 6
- II. Electron Microscopy 7

### OPTICAL PROPERTIES

- I. Transmission and Reflectivity Measurements 9
- II. Modulated Reflectivity 10
- III. Photoconductivity 11
- IV. Photoemission 12

### TRANSPORT PROPERTIES

- I. Resistivity vs. Temperature 14

### REFERENCES 15

### FISCAL STATUS 17

### APPENDICES 18

### Summary

A continuing effort is being made to maintain a closely knit experimental and theoretical program. Theoretical work on the use of Hermite functions to compute Hilbert (Kramer Kronig) transforms is completed and has been successfully tested on several systems and applied to the analysis of optical data on single crystalline and amorphous thin films of  $\text{Sb}_2\text{Se}_3$ .

A satisfactory method of preparing thin amorphous films of controlled composition by coevaporation has been developed and improved upon in the past six months. Differential thermal analysis has yielded important information on the compositional dependence of the glass to crystalline transition in  $\text{Sb}_x\text{Se}_y$  amorphous films.

Mossbauer studies have yielded important information on the short range order of amorphous films and on the structural chemistry of mixed chalcogenide systems. This technique, where applicable, appears to fulfill a need for analysis on a microscale where more conventional analytical tools such as X-ray and electron microscopy are inadequate. However, initial studies of  $\text{Sb}_x\text{Se}_y$  amorphous films by electron microscopy are yielding very interesting data but a full interpretation of the data awaits compositional analysis of the films.

In the optical studies of thin amorphous films, one of the more significant findings has been the close correspondence between the energy band gaps in the crystalline and amorphous form of  $\text{Sb}_2\text{Se}_3$  and the apparent lack of band tailing. Further optical measurements on single crystal  $\text{Sb}_2\text{Se}_3$  in the neighborhood of the band edge as a function of crystal orientation

have supported the initial findings of a direct transition. We are currently pressing ahead with resistivity versus temperature measurements on both the amorphous and single crystal forms to obtain thermal activation energies for comparison with the optical values.

Several different approaches to modulated reflectivity (and modulated absorption) are under development. This data should prove invaluable in the analysis of the electronic structure of the antimony chalcogenides. Along the same lines, the setting-up of apparatus for the very powerful technique of photoemission is at a final stage of completion and is already yielding results on the density of states.

As evidenced by the large number of references to Bull. Am. Phys. Soc. much of the work is still in the initial stages. In keeping with past practice we have included preprints of work currently being submitted for publication to elaborate, for the interested reader, on details not suitable for this general progress report. A summary of the more significant findings of this program to date will be presented at the forthcoming International Symposium on Amorphous and Liquid Semiconductors and an abstract is appended to this report. Reprints of papers, published since the last six-monthly report, are also appended.

## THEORETICAL RESEARCH

### I. The Kramers-Kronig (Hilbert) Transform

During the last six months the work initiated earlier on the use of Hermite functions to compute Hilbert (Kramers-Kronig) Transforms has been completed. A paper outlining the general mathematical technique has been submitted for publication and a preprint was included in the previous technical report. This paper concentrates upon the application of the method to functions of compact support such as densities of states. Hilbert Transforms of such functions are useful, e.g., in the computation of optical functions from the results of electronic structure calculations. Briefly, a convergent, matrix representation of the Hilbert Transform kernel has been employed to compute Hilbert Transforms of two densities of states, 1) the classic simple cubic s-band (triple cosine) density of states and 2) the electronic density of states of fcc palladium<sup>1</sup>. The results indicate that critical point structure does not shift in frequency under a proper Hilbert Transform. Details of the computational method and its analytical development are found in the paper.

The application of the above technique to optical data analysis, i.e., to the extraction of optical functions from experimental near-normal incidence reflectivity measurements has also come to fruition. A preprint of a paper which is now in its final stages of preparation is attached to this report as Appendix A. A preliminary report of the results of the technique as applied to  $\text{Sb}_2\text{Se}_3$  crystalline samples was presented at the March Meeting of the American Physical Society in Cleveland<sup>2</sup>(Appendix B). Further application of the technique has been made to thin amorphous films

of the composition  $\text{Sb}_2\text{Se}_3$  and this work was reported at the April Meeting of the American Physical Society in Washington<sup>3</sup>(Appendix C). There are indications of substantial differences in the structural details of the optical functions of crystalline and amorphous  $\text{Sb}_2\text{Se}_3$ . Further investigations in this area are underway. Basically the method employs the reflectivity of systems of simple charged oscillators to extrapolate the experimental data outside the measured data range and to convert the function whose Hilbert Transform needs to be computed to one of compact support. The methods employed in the previous work described above are then applicable. As a check upon the power of the technique it has been applied to reflectivity data<sup>4</sup> on  $\text{BaF}_2$  in the far ultraviolet. This data has a wealth of sharp structure arising, most likely, from deep excitons and provides a test of the resolution of the computational technique.

## II. Electronic Structure

Some progress has been made on the computation of the electronic spectra of amorphous materials. The method we have explored is similar in spirit to the work of Maschke and Thomas<sup>5</sup> for electronic structure in amorphous solids with short-range order. We are planning to apply our method to specific amorphous solids. A computer program to compute electronic energies of a model of amorphous Ge and the associated density of states, is under development. The computational problems are severe both as to complexity and as to computational time required. The problem is, however, tractable and with continuing work will be completed.

In another vein work has been initiated to attempt to make use of the results recently obtained by Romeris<sup>6</sup> to connect the electronic structure of amorphous solids to that of crystals of similar composition.

Romeris has shown that critical point structure behaves in a particular manner as a "crystal" potential varies from being truly periodic to being almost periodic. Since there is evidence<sup>3</sup> of critical point structure in the optical functions found for amorphous films of  $\text{Sb}_2\text{Se}_3$  it may be feasible to correlate this structure in a definite manner with that found in crystalline  $\text{Sb}_2\text{Se}_3$ . We have, therefore begun to explore methods for tracking the behavior of critical point structure with disorder.



## MATERIALS RESEARCH

### I. Amorphous Thin Films

A large number of amorphous films of various compositions in the Sb-Se system have now been prepared by coevaporation. The compositions were determined by micro-probe analysis in conjunction with the Geophysical Laboratory of the University of Chicago. A fair degree of reproducibility has been obtained but, because of the critical dependence of optical properties on composition<sup>7</sup> (Appendix B) the deposition controllers (Sloan Omni IIA) have had to be upgraded. The most significant improvements are: newly-developed circuit boards have been installed, gold-plated quartz crystals of circular geometry are now employed and, most importantly, the frequency and deposition rate of each source is continuously monitored externally by chart recorders throughout deposition. Despite these improvements control of stoichiometry to within 1 atomic percent cannot be guaranteed.

In an attempt to obtain even closer control of composition two further approaches will be tried: 1) sputtering, under equilibrium conditions; 2) coevaporation of a graded composition across an extended substrate. Both systems are under construction, the former being nearly completed.

### II. Crystalline Thin Films

The three-temperature technique<sup>8</sup> was successfully applied to the deposition of a stoichiometric, polycrystalline film of  $\text{Sb}_2\text{Se}_3$ . There were difficulties in achieving adequate deposition rates which are determined by both substrate temperature and melt temperature. Too fast

a deposition rate produced a film with small, irregular crystal grains. With too slow a rate there is virtually no deposition. It was found that a fused-quartz substrate temperature of  $450^{\circ}\text{C}$  and a melt temperature of  $630^{\circ}\text{C}$  produced a satisfactory film for optical studies.

### III. Single Crystals

A new single crystal growth apparatus is under development using a tin-oxide coated quartz tube for both the background heating elements and the zone heating element. These tubes have the advantage that they will develop temperatures well above  $600^{\circ}\text{C}$  while remaining very transparent to allow good visibility of the molten zone and hence good control of the growth process.

### IV. Differential Thermal Analysis

DTA measurements have been carried out on various compositions of Sb-Se films in the temperature range of  $30^{\circ}\text{C}$  to  $300^{\circ}\text{C}$ <sup>9</sup> (Appendix C). The glass to crystalline phase transitions of the samples were investigated. This transition was found to be endothermic and located at  $\sim 190^{\circ}\text{C}$  for  $\text{Sb}_2\text{Se}_3$ . Those films that were on the Se-rich side of  $\text{Sb}_2\text{Se}_3$  showed amorphous-crystalline transition for Se, which was located at  $\sim 120^{\circ}\text{C}$ , as well as the  $\text{Sb}_2\text{Se}_3$  transition. Plans have been made to incorporate a more sensitive arrangement of thermo-couples more suited to a thin film geometry.

## STRUCTURAL INVESTIGATIONS

### I. Mossbauer Studies

Work performed in collaboration with Dr. S. Ruby of Argonne National Laboratory produced the very significant finding that all Sb atoms in  $\text{Sb}_x\text{Se}_y$  (including  $\text{Sb}_2\text{Se}_3$ ) amorphous solids sit in closely similar environments in contrast to the  $\text{Sb}_2\text{Se}_3$  crystal where there are two distinct sites<sup>10</sup> (Appendix B). This is of particular significance in that it lends support to the view that the evaporated films are in reality amorphous and not "micro-crystalline", since we now know that the short-range-order differs in the two forms. This work will be submitted for publication and a preprint is attached (Appendix D).

In order to investigate cross-linking effects of Group IV elements in amorphous Group V chalcogenides, Mossbauer studies using  $^{119}\text{Sn}$  in a  $\text{BaSnO}_3$  source, have been carried out on  $\text{Sn}_x(\text{As}_2\text{Se}_3)_{1-x}$  glasses with varying concentrations of tin, i.e. ( $x = 2.5, 5.0, 8.0, 10.0$  At. %) and on the two crystalline samples of  $\text{SnSe}_2$  at liquid nitrogen and liquid He temperatures<sup>11</sup> (Appendix B).  $\text{Sn}_x(\text{As}_2\text{Se}_3)_{1-x}$  glasses samples were prepared by quenching the melts into a brine bath at 200K.

The limit of tin solubility in the quenched glassy state is tentatively set by Kolomiets et al<sup>12</sup> at 7 At. %. Thus 8.0 and 10.0 At. % Sn, glass samples may have a crystalline component. X-ray patterns for all the samples, however, were similar and characteristic of amorphous systems. The major phase present in a deliberately crystallized  $\text{As}_2\text{Se}_3 + 10$  At. % Sn sample is  $\text{SnSe}$  and the corresponding amorphous sample also contains a

small amount of SnSe. A critical Mossbauer spectra for 10 At. % Sn amorphous sample at 4.2<sup>0</sup>K shows an increase of absorption by about 15% compared to that at liquid nitrogen temperature. The overall character of the spectra is similar to that obtained by Borisova et. al.<sup>13</sup>, the major difference occurred in the intensities of the spectra corresponding to SnSe<sub>2</sub> and SnSe. The average shift in all systems corresponding to SnSe<sub>2</sub> is 1.68 mm/sec which is slightly less than that of  $\alpha$ -Sn. On the basis of Ruby's<sup>14</sup> atomic calculations, the electronic configuration is 0.7s, 3.3p. The average shift corresponding to SnSe is 3.45 mm/sec and the electronic configuration turns out as 1.6s, 2.4p.

Thus, it is clear from the present Mossbauer investigations of the amorphous systems that the degree of local order is very high, i.e., molecules or microcrystals of small enough dimensions to escape x-ray detection are held in a disordered matrix. The microchemistry does appear to correspond to the suggested chemistry of Shkolnikov<sup>15</sup>. The Mossbauer spectra for Sn in the glasses corresponds very closely to those of crystalline SnSe and SnSe<sub>2</sub>. However the range of chemical order is too small to be detected by x-ray diffraction.

## II. Electron Microscopy

Electron microscopy and electron diffraction studies were made on thin (about 250<sup>0</sup> Å thick) films of Sb<sub>x</sub>Se<sub>y</sub>. Amorphous films appear granular with irregularly shaped particles of about  $1 \times 10^{-4}$  cm diameter. The corresponding diffraction pattern consists of three diffuse bands. One can observe crystal growth from these amorphous films as caused by the heat of the electron beam. Depending on the sample composition, different types of ordering are observed: 1) bizarre looking dendrite-like

needles of about  $1000 \text{ \AA}$  width with a complicated fine structure, 2) fibres of about  $60 \text{ \AA}$  width which are lined up parallel to one another or are spiralling around each other, 3) rounded domains of micron size with narrow subdomains of about  $100 \times 1000 \text{ \AA}$  which have different alignments for different domains.

The diffraction patterns of sections  $50 \mu$  in diameter of the crystallized films range from spotty powder patterns and fibre patterns to single crystal patterns. Typical is a one dimensional ordering resulting in irregularly spaced spots on equally spaced lines. The ordered dimension varies somewhat around  $3.24 \text{ \AA}$ . It is not known at this date if the corresponding reflections relate to the "forbidden" (100) and (010) reflections from  $\text{Sb}_2\text{O}_3$  structure or belong to a completely new crystal type. Definitely not compatible with the  $\text{Sb}_2\text{O}_3$  structure are recurring hexagonal patterns which cannot be attributed either to selenium or antimony.

A complete interpretation of the results will be attempted when all the sample compositions have been analyzed.

## OPTICAL PROPERTIES

### I. Transmission and Reflectivity Measurements

Several different methods have been employed to determine the optical constants  $n$  and  $k$ , from the reflectivity ( $R$ ) and transmission ( $T$ ) of a thin film in the spectral region near and below the absorption edge. The first technique tried was to search the  $n$ - $k$  plane for points that would fit the observed  $R$  and  $T$ . This method had limited success because for a given  $R$  and  $T$  there are multiple solutions in the  $n$ - $k$  plane and the computer program was taking excessive time. The other method tried was that of quadratic interpolation. This method is not yet fully completed, but it gives greater accuracy in less computer time.

Absorption constant ( $\alpha$ ) vs. photon energy graphs were determined by transmission and reflectivity data for a wide range of compositions of Sb-Se amorphous films<sup>7</sup> (Appendix B). A close correspondence was noted between the position of the optical gap of the amorphous films and single crystal  $\text{Sb}_2\text{Se}_3$ . The  $\alpha$  values were determined from  $10^6\text{cm}^{-1}$  to  $10^3\text{cm}^{-1}$  for selected samples using a wide variation of sample thicknesses. Thin films ( $\sim 5_\mu$ ) of  $\text{Sb}_2\text{Se}_3$  must still be made and measured in order to determine the type of transition that occurs (direct or phonon assisted).

The reflectivity and transmission of single crystals of  $\text{Sb}_2\text{Se}_3$  grown in a horizontal zone refiner were measured in the range 0.03 eV to 11 eV<sup>16</sup> (Appendix B).  $R$  and  $T$  were measured as a function of polarization in the cleavage plane. The reflectivity structure was shown to

agree with Soblov et. al.<sup>17</sup> for the two polarization directions in the cleavage plane in the energy range 1 eV to 4 eV; and for unpolarized light in the range 4-11 eV. The energy range 0.03 to 0.5 eV was covered on the Beckman IR-12 spectrophotometer; 0.5-4 eV on a Cary 14 R spectrophotometer; and 4-11 eV on a McPherson vacuum U.V. spectrophotometer at Argonne National Laboratory (kindly loaned by Dr. P. Yuster). The absorption coefficient was calculated from this data near the absorption edge at about 1 eV. Different powers of the absorption coefficient were plotted versus wavelength to obtain the type of transition responsible for the absorption edge. A direct allowed transition was found for both directions of polarization.

Initial low light level measurements have been made using an S.S.R. photon counter. Great lengths have been gone to in order to prevent light leaks in the system. The phototubes can be cooled down to solid CO<sub>2</sub> temperatures for operation in a low noise mode. This arrangement should prove to be quite valuable for the measurement of optical transmission well above the absorption edge and also for small signal modulation experiments.

## II. Modulated Reflectivity

Thermally modulated reflectivity measurements were performed on single crystals of Sb<sub>2</sub>Te<sub>3</sub> with the light incident on the cleavage plane ( $E \perp C$ )<sup>18</sup> (Appendix C). The data was taken in the visible and near infrared regions and was found to agree with critical points observed in the transmission spectrum of thin cleaved sample using a photon counter.

Electro-reflectance apparatus is now completed which will be used

to measure the electro-modulated reflectivity spectrum of  $\text{Sb}_2\text{Se}_3$  single crystals, in all three orientations of the electric vector, and amorphous  $\text{Sb}_x\text{Se}_y$  films.

Also under construction is apparatus for wavelength modulated reflectivity which involves halving the optical beam from the exit slit of a monochromator and comparing the reflectivity of the sample to light from the two halves by means of a lock-in amplifier.

Construction of apparatus for rotoreflectance is also underway. This technique utilizes a rotating polarizer to measure the changes in reflectivity as a function of electric vector orientation.

### III. Photoconductivity

In the photoconductivity area most work was concentrated on study of amorphous  $\text{Sb}_x\text{Se}_y$ . The spectral dependence of photoresponse and photoconductive gain depend critically on sample composition. The photoconductivity activation energy (as determined by Moss'<sup>19</sup> criterion) generally agrees with the optical activation energy as determined from transmission measurements<sup>7</sup> (Appendix B) in case of stoichiometric amorphous  $\text{Sb}_2\text{Se}_3$  being equal to 1.1 eV, which is very close to that of single crystalline  $\text{Sb}_2\text{Se}_3$ . We feel that this point is of fundamental importance as it shows that the gap is approximately the same in amorphous and crystalline  $\text{Sb}_2\text{Se}_3$ ; contrary to previously published work by Kolomiets et. al.<sup>20</sup> whose results were probably affected by deviations from stoichiometry. The effect of trapping states inside the forbidden gap on photoconductive gain and on the response time was investigated using a dc light "bias" of variable intensity to fill traps to any desired degree.

In order to provide meaningful comparison of the photoconductive



properties of amorphous  $\text{Sb}_2\text{Se}_3$  with single crystalline  $\text{Sb}_2\text{Se}_3$ , a detailed investigation of the photoconductive properties of the single crystalline phase was performed<sup>21</sup> (Appendix B). The onset of photoconductivity was found to depend on orientation of electrical vector  $E$  of polarized light with respect to three principal crystallographic axes in agreement with dependence of optical absorption on the above parameters.

An interesting feature of the photoconductive kinetics of  $\text{Sb}_2\text{Se}_3$  is a rather long response time - even in the region of fundamental absorption the response time is of the order of 250-300 micro-seconds, which can be explained only by strong trapping effects which obscure the surface recombination. This long response time probably also gives rise to photosensitivity over wide spectral range (1-3 eV).

So far, we are able to make the following conclusions: The spectral response, particularly the activation energy of amorphous stoichiometric  $\text{Sb}_2\text{Se}_3$  is very similar to that of single crystal  $\text{Sb}_2\text{Se}_3$ . The onset of photoconductivity in amorphous  $\text{Sb}_2\text{Se}_3$  is at least that sharp as in the case of the single crystal modification, a fact which seems to be contradictory to effects of band tailing as found by Weiser and Brodsky<sup>22</sup> for amorphous  $\text{As}_2\text{Te}_3$ . Also the response time and photosensitivity is at least two orders of magnitude lower than that in the crystalline phase indicating, together with the previous findings, that trapping states at band edges in amorphous phase of  $\text{Sb}_2\text{Se}_3$  seem to be electrically much less effective than in the single crystal phase.

#### IV. Photoemission

Construction of a ultrahigh vacuum ( $10^{-10}$  -  $10^{-11}$  torr) phototube

has been completed together with provision for sample cleaving in situ. Presently, an attachment is under construction for the evaporation of amorphous Sb-Se films in situ.

Also completed is the whole detection and electronic circuit employing a retarding field detector. A few preliminary runs show that the apparatus, i.e., McPherson 225 Vacuum UV Monochromator, all vacuum parts and all electronic equipment, is in good working condition and initial density of states curves have been recorded. These curves will be compared with density of states from band structure calculations for amorphous and crystalline  $\text{Sb}_2\text{Se}_3$ . In order to obtain better resolution of transitions at critical points in Brillouen zone partially obscured by phonon broadening and by the absorptive background, first and second derivatives of the density of states vs. energy will be also recorded simultaneously. For this purpose doublers and triplers of the modulation frequency have been constructed.

## TRANSPORT PROPERTIES

### I. Resistivity vs. Temperature

Work has progressed in the low temperature measurement of very high resistance ( $\sim 10^{11}$  ohms) thin films. These measurements have been carried out in a "Cryotip", which uses the Joule-Thompson expansion of He and H<sub>2</sub> to provide temperatures from ambient to 4.2°K. A four-probe configuration of evaporated gold contacts is used to minimize contact resistance. The main problems encountered thus far are those of vacuum integrity, shielding of circuits and ground loops between circuits. These have been solved to the extent that a standard resistance of the same order of magnitude as the film has been measured in the apparatus.

# REFERENCES

1. F. M. Mueller, A. J. Freeman, J. O. Dimock, and A. M. Furdyna, Phys. Rev. (in press).
2. Shaffer, J.C., and Afshar, R., Bull. Am. Phys. Soc., 16, 374 (1971).
3. Shaffer, J.C., Afshar, R., Wood, C., and Mueller, R., Bull. Am. Phys. Soc., 16, 519 (1971).
4. Rubloff, G.W., Freeouf, J., Fritzche, H., and Morase, K., Phys. Rev. Ltrs., 26, 1317 (1971).
5. Maschke, K. and Thomas, P., Phys. Stat. Sol. 39, 453 (1970).
6. Romeris, M.V., J. Math. Phys. 12, 552 (1971).
7. Wood, C., Mueller, R., Gilbert, L.R., Hurych, Z. and Wang, C.C., Bull. Am. Phys. Soc. 16, 305 (1971).
8. Gunther, K.G., Compound Semiconductors 1, Ed. Willardson and Goering (Reinhold, 1962).
9. Gilbert, L.R., and Wood, C., Bull. Am. Phys. Soc. 16, 500 (1971).
10. Ruby, S.L., Gilbert, L.R., and Wood C., Bull. Am. Phys. Soc. 16, 303 (1971).
11. Taneja, S.P., Gilbert, L.R., Harper, W.C., Kimball, C.W., and Wood, C., Bull. Am. Phys. Soc. 16, 303 (1971).
12. B.T. Kolomiets et. al. Collection: The Glassy State. Izd. Akad. Nauk. USSR, Moscow (1960) p. 456.
13. Z.U. Borisova et. al. Sov. Phys. - Semiconductors 4, 443 (1970).
14. S.L. Ruby, Mossbauer effect Methodology, vol. 3, Ed. I.J. Gruverman, 1967 p. 203.
15. E.V. Shkol'nikov, Solid State Chemistry ed. Z.U. Borisova. (consultants Bureau, N.Y. 1966), p. 142.
16. Van Pelt, B., and Wood. C., Bull, Am. Phys. Soc. 16, 306 (1971).
17. Sobolev, V.V., Shutov, S.D., Popov, Y.V. and Shest'atskii, S.N., Phys. Stat. Sol. 30, 349 (1968).
18. Wood, C., Hurych, Z., and Van Pelt, B., Bull. Am. Phys. Soc. 16, 652 (1971).

19. Moss, T.S., Photoconductivity in the Elements
20. Kolomiets, B.T., Lyubin, V.M., and Tarkin, D.V., Sov. Phys. Sol. State 1, 819 (1959).
21. Hurych, Z. Wang, C.C. and Wood, C., Bull. Am. Phys. Soc. 16, 400 (1971).
22. Weiser, K., and Brodsky, M.H., Phys. Rev. B1, 791 (1970).

FISCAL STATUS

	<u>Amount Budgeted</u>	<u>Amount Expended May 31, 1971</u>
Personnel	\$31,368.00	\$30,741.00
Supplies, Expenses & Services	12,800.00	11,004.00
Travel	2,500.00	2,268.00
Indirect Costs	11,952.00	11,952.00

## **APPENDIX A**

**APPENDIX A**

**A NEW METHOD FOR THE KRAMERS-KRONIG ANALYSIS OF OPTICAL DATA\***

**R. Afshar**

**Northern Illinois University, DeKalb, Illinois**

**F. M. Mueller**

**Argonne National Laboratory, Argonne, Illinois  
and**

**Northern Illinois University, DeKalb, Illinois**

**and**

**J. C. Shaffer**

**Northern Illinois University, DeKalb, Illinois**

**\*This work was performed under the auspices of the Atomic Energy Commission and was supported by the Advanced Research Projects Agency of the Department of Defense and was monitored by the Army Research Office, Durham under Contract No. DA-ARO-D-31-124-70-G77.**



ABSTRACT

Herein a new technique for performing Kramers-Kronig (Hilbert) transforms upon experimental normal incidence reflectivity data is presented. The method is based upon development of the Hilbert principal value kernel and suitably defined functions closely related to the data in the space of Hermite functions. Well defined procedures for extrapolating the data into unmeasured regions of the spectrum are employed.

The method is applied to reflectivity data taken on two solids and the results are analyzed as to their reliability as is the general utility of the technique. An important conclusion drawn from the results is the invariance of the location of critical point structure under the Kramers-Kronig transform. Some of the details of the numerical procedures and their convergence are also briefly discussed.

## I. INTRODUCTION

Great progress has been made in extending the frequency region over which the optical spectroscopy of solids is regularly performed. It is presently relatively commonplace for measurements of, e.g., near-normal incidence reflectivity, to be carried out from far infra-red through vacuum ultra-violet frequencies. Reflectivity measurements on bulk single crystals over wide spectral ranges are made especially valuable by the possibility of performing a Kramers-Kronig analysis upon the data to obtain the phase of the complex reflectivity and hence all of the optical functions of a given material. This general procedure has been adopted by many workers<sup>(1-4)</sup> and several computational techniques have been developed for carrying out the requisite integral transforms. In Section II these are briefly and critically reviewed. Also in that section the method we have employed in this work is outlined. The general procedure has been separately detailed in a somewhat different context<sup>(5)</sup> and so the intent here is to concentrate upon those aspects of Kramers-Kronig analysis and of our method which are specific to the analysis of optical data.

In Section III the results of the application of this new method to normal incidence reflectivity data on  $\text{Sb}_2\text{Se}_3$ <sup>(6)</sup> and  $\text{BaF}_2$ <sup>(7)</sup> single crystals are presented. The reflectivity data in these two cases were measured over different spectral regions and, additionally, the two sets of data are quite different in structural detail. They thus provide tests of somewhat different

## APPENDIX A

- 4 -

character (e.g., as to resolution) for the technique.

In Section IV an analysis of the accuracy, reliability, and systematic use of the method is given. Studies of the convergence of the necessary numerical expansion procedures are presented as<sup>16</sup> a discussion of some general conclusions on the characteristics of the Hilbert transform as it relates to the optical properties of solids. Possible applications to other problems in solid state physics are considered.

### II. THE KRAMERS-KRONIG (HILBERT) TRANSFORM

#### APPLIED TO OPTICAL DATA

If it were possible to measure the (near-normal incidence) fractional coefficient of reflected intensity, or reflectance,  $R(\omega)$ , of a bulk solid sample (for a given orientation and polarization) in vacuo (air) for all frequencies then the phase of the complex (amplitude) reflection coefficient  $\hat{r}(\omega) = R^{1/2}(\omega)e^{i\varphi(\omega)}$  could be determined from the Kramers-Kronig dispersion relation<sup>(8)</sup>

$$\varphi(\omega) = \frac{P}{\pi} \int_{-\infty}^{+\infty} \frac{\ln r(\omega') d\omega'}{\omega' - \omega} \quad (1)$$

where  $r(\omega') = R^{1/2}(\omega')^*$ , and  $R(\omega)$  has been extended to negative

\*Most often dispersion relations are derived for the real and imaginary parts of complex causal response functions which of a real variable must be of class  $L^2(-\infty, \infty)$ . However such relations can also be derived for the phase and logarithm of the modulus of complex functions for which  $\lim_{\omega \rightarrow \infty} r(\omega) \rightarrow 0$  at least as rapidly as

$\omega^{-n}$  where  $n > 1$ . Thus although the logarithm of the reflectivity is not  $L^2(-\infty, +\infty)$  a dispersion relation exists between it and the phase. For causal response functions the real and imaginary parts are each of class  $L^2(-\infty, \infty)$ . An excellent discussion of these points is given in Ref. (8).

# APPENDIX A

- 5 -

frequencies as an even function. Knowledge of  $R(\omega)$  and  $\varphi(\omega)$  is tantamount to knowledge of all the optical functions since  $\hat{n}(\omega) = n(\omega) + i\kappa(\omega)$  is related to the complex reflection coefficient by

$$\hat{n}(\omega) = (1 + \hat{r}(\omega))/(1 - \hat{r}(\omega)) \quad , \quad (2)$$

a simple homographic transformation. Given  $\hat{n}(\omega)$ ;  $\hat{\epsilon}(\omega)$ , the complex dielectric function, and the energy loss function,  $\text{Im}[\hat{\epsilon}^{-1}(\omega)]$ , are easily obtained.

There are two paramount difficulties in Eq. (1) which must be overcome in order that this data reduction be effected. In the first place data is never available for all frequencies due to the finite frequency cutoff of real spectrometers. Secondly the kernel of the Hilbert transform in Eq. (1) is highly singular and, in fact, that equation is most properly regarded as a functional and the kernel as a generalized function. A casual numerical attack upon it or any of its equivalents can be rather precarious particularly in its effect upon the critical point structure exhibited by the spectrum under consideration.

It is useful to review some of the methods which have been employed to deal with the aforementioned problems. Generally the first problem, that of finite data ranges has been handled by extrapolating the data into unmeasured regions. Above the highest frequency the data is usually extended using one or more terms of a Lavrent series. Unless great care is taken this may introduce spurious structure into the spectrum. Below the lowest frequency measured the data is normally extrapolated

## APPENDIX A

- 5 -

frequencies as an even function. Knowledge of  $R(\omega)$  and  $\phi(\omega)$  is tantamount to knowledge of all the optical functions since  $\hat{n}(\omega) = n(\omega) + i\kappa(\omega)$  is related to the complex reflection coefficient by

$$\hat{n}(\omega) = (1 + \hat{r}(\omega))/(1 - \hat{r}(\omega)) \quad , \quad (2)$$

a simple homographic transformation. Given  $\hat{n}(\omega)$ ;  $\hat{\epsilon}(\omega)$ , the complex dielectric function, and the energy loss function,  $\text{Im}[\hat{\epsilon}^{-1}(\omega)]$ , are easily obtained.

There are two paramount difficulties in Eq. (1) which must be overcome in order that this data reduction be effected. In the first place data is never available for all frequencies due to the finite frequency cutoff of real spectrometers. Secondly the kernel of the Hilbert transform in Eq. (1) is highly singular and, in fact, that equation is most properly regarded as a functional and the kernel as a generalized function. A casual numerical attack upon it or any of its equivalents can be rather precarious particularly in its effect upon the critical point structure exhibited by the spectrum under consideration.

It is useful to review some of the methods which have been employed to deal with the aforementioned problems. Generally the first problem, that of finite data ranges has been handled by extrapolating the data into unmeasured regions. Above the highest frequency the data is usually extended using one or more terms of a Lavrent series. Unless great care is taken this may introduce spurious structure into the spectrum. Below the lowest frequency measured the data is normally extrapolated

# APPENDIX A

- 6 -

using a Taylor series. Knowledge of the static dielectric constant of the material being studied can make this a most reasonable procedure. The singular kernel in (1) is usually handled by transforming (1) into the equally valid form

$$\varphi(\omega) = \frac{2\omega}{\pi} \int_0^\infty \frac{\ln \rho(\omega') - \ln \rho(\omega)}{\omega'^2 - \omega^2} d\omega' \quad (3)$$

The inclusion of a small additional part in the denominator of (3),  $\eta^2$ , is then justified by the principal value character of (1) and if it is chosen sufficiently small the finite arithmetic character of digital computation allows the transform to be carried out in an approximate manner. It is interesting to examine in more detail the methods used by some of the workers who have attacked the Kramers-Kronig transform in optical problems. INSPI

In another publication<sup>(5)</sup> (hereafter denoted I) the suitability of the Hermite functions (harmonic oscillator eigenfunctions) as a basis set for accomplishing Hilbert transforms has been demonstrated. The interest there was in the Hilbert transforms of electron (or phonon) densities of states and thus the functions to be transformed were of compact support, i.e., they vanished outside some finite range on the real line, and were bounded. In the application of Kramers-Kronig analysis to reflectivity data these characteristics are not present however as will be shown suitable treatment of the data brings the problem into a form amenable to the methods described in I.

In I it is shown that if a function  $\alpha(\omega)$  have a convergent Hermite expansion

# APPENDIX A

-7-

$$\alpha(\omega) = \sum_n \alpha_n \phi_n(\omega) \quad (4)$$

where the  $\phi_n(\omega)$  are the Hermite functions, then its Hilbert transform partner  $\beta(\omega)$  also has a Hermite expansion

$$\beta(\omega) = \sum_n \beta_n \phi_n(\omega) \quad (5)$$

where

$$\beta_n = \sum_m S_{nm} \alpha_m, \quad (6)$$

$S_{nm}$  being a compact matrix representation of the Hilbert transform "operator" in the space of Hermite functions.\*  $S_{nm}$  vanishes unless  $n + m$  is odd and, for integer  $h$ , may be written

$$S_{nm} = (-1)^{h+1} S'_{nm}; \quad h = (m-n-1)/2 \quad (7)$$

Computation of the matrix elements  $S'_{nm}$  is most easily accomplished as in I; from

$$S'_{nm} = \int_{-\infty}^{+\infty} dt \operatorname{SGN}(t) \phi_n(t) \phi_m(t). \quad (8)$$

---

\* It can be shown (8) that causal complex response functions which are the simplest class of functions whose real and imaginary parts are Hilbert transform pairs are necessarily square integrable as are their real and imaginary parts separately. (8) However the class of square integrable functions does not exhaust all possible Hilbert transform pairs (consider  $\phi(\omega)$  and  $\ln r(\omega)$  in (1)). The Hermite decomposition of the Hilbert transform can be directly applied only to the square-integrable case because of the need for convergent Hermite expansions to exist.

## APPENDIX A

- 8 -

The matrix elements are then computed by using the Hermite integration technique, as detailed in (I).

Direct application of this technique to (1) is obviated since as  $\omega \rightarrow \pm \infty$   $r(\omega) \rightarrow 0$ , hence  $\ln r(\omega) \rightarrow -\infty$  as  $\omega \rightarrow \pm \infty$ . The function  $\ln r(\omega)$  is therefore not a square integrable function and has no convergent expansion in Hermite functions. A simple procedure however removes this difficulty allowing the full power of the Hermite analysis to bear upon the structure in the optical problem as well as providing a self consistent extrapolation of the data into unmeasured regions. Since the Hilbert transform (1) is a linear integral transform portions of  $\ln r(\omega)$ , the transforms of which are closed-form analytic functions, can be removed leaving a residual function whose transform must be attacked numerically. The portions removed are chosen so that they smoothly fit to  $\ln r(\omega)$  itself near the boundaries of measurement and furthermore give reasonable extrapolations of  $\ln r(\omega)$  into the unmeasured regions. Thus (1) becomes

$$\varphi(\omega) = \varphi_0(\omega) + \theta(\omega) \quad (9)$$

where

$$\varphi_0(\omega) = \frac{P}{\pi} \int_{-\infty}^{+\infty} \frac{g(\omega')}{\omega' - \omega} d\omega' \quad (10)$$

where  $g(\omega)$  is the function which was used to fit  $\ln r(\omega)$  near the boundaries of measurement and to extrapolate into the unknown regions.  $g(\omega)$  should be chosen from among functions with known analytic Hilbert transforms  $\varphi_0(\omega)$ . If we denote  $\ln r(\omega) - g(\omega)$



# APPENDIX A

- 9 -

by  $\Delta(\omega)$  then

$$\theta(\omega) = \frac{P}{\pi} \int_{-\infty}^{+\infty} \frac{\Delta(\omega') d\omega'}{\omega' - \omega} \quad (11)$$

By construction  $\Delta(\omega')$  is a compact function which is, in practice, also bounded. It is, therefore, square integrable and the Hermite analysis technique can be used to compute  $\theta(\omega)$ . It is then only necessary to choose appropriate  $g(\omega)$ . Our procedure has been as follows. The dielectric constant or index of refraction of a system of classical charge oscillators with given resonant frequencies, damping constants, and oscillator strengths  $\rightarrow$  is well-known. For example, the index of refraction can be approximated (for a dilute gas of  $G$ ach oscillators) as

$$n(\omega) = 1.0 + \sum_i \frac{v_i}{(\omega_i^2 - \omega^2) + i\Gamma_i \omega} \quad (12)$$

in which the  $\omega_i$  are the resonant frequencies, the  $\Gamma_i$  the damping constants (linewidths) and the  $v_i$  essentially the oscillator "strengths". The complex amplitude reflection coefficient of a bulk sample of material with this  $\hat{n}$ , is

$$p_o(\omega) e^{i\varphi_o(\omega)} = \hat{p}_o(\omega) = (\hat{n}(\omega) - 1)/(\hat{n}(\omega) + 1) \quad (13)$$

By adjusting the various parameters in (12) we can find an  $\hat{n}(\omega)$  for which the resulting  $\ln \hat{p}_o(\omega)$  will smoothly and closely approximate  $\ln r(\omega)$  near the data boundaries. The same function (13) provides a natural choice of extrapolation of  $r(\omega)$  and hence  $\ln r(\omega)$  into

# APPENDIX A

- 10 -

the unmeasured regions.  $\varphi_0(\omega)$ , the analytic portion we have extracted from the total Hilbert transform is then given by

$$\varphi_0(\omega) = \tan^{-1} \frac{2 \kappa(\omega)}{n_0^2(\omega) + \kappa_0^2(\omega) - 1} \quad (14)$$

where, of course,  $n_0(\omega)$  and  $\kappa_0(\omega)$  are the real and imaginary parts of  $\hat{n}_0(\omega)$ . For the data analyzed in this contribution we have found that choosing two frequencies for classical oscillators and adjusting the other parameters ( $\Gamma_1, \Gamma_2, \nu_1, \nu_2$ ) allows us to obtain a sufficiently smooth fit to the data in the relevant regions. Note that  $R(\omega) = |r(\omega)|^2$  has a dominant  $\omega^{-4}$  dependence at sufficiently high frequencies in the extrapolation here employed. The entire data analysis problem has now been reduced to the computation of Hermite expansion coefficients of  $\Delta(\omega)$  and matrix multiplication of these to generate the expansion coefficients of  $\theta(\omega)$ . The next section is devoted to the details of the procedure we have described as it has been applied to data on  $\text{Sb}_2\text{Se}_3$  and  $\text{BaF}_2$  single crystals.

## APPENDIX A

-11-

### III. APPLICATION TO REAL SOLIDS

#### A. Optical Functions of $\text{Sb}_2\text{Se}_3$ .

$\text{Sb}_2\text{Se}_3$ , in crystalline form, has an orthorhombic lattice with a rather complex unit cell containing four units of  $\text{Sb}_2\text{Se}_3$  with two non-equivalent sites both for the antimony and selenium atoms. The space group is  $D_{2h}^{16}$  (Pnma). The optical functions are anisotropic, however, in this work we ignore that fact as it is not pertinent to our purpose of illustrating the use of our method of Kramers-Kronig analysis. In Fig. 1 is shown the reflectivity to unpolarized light, in the frequency range 1.5eV to 11.0eV, of a cleavage plane of  $\text{Sb}_2\text{Se}_3$  as measured by Wood<sup>6</sup> et al. This data is in close agreement with the data of Shutov<sup>9</sup> et al in overlapping measured regions of the spectrum. The data, as may be seen, indicates an absorption edge near 1.0eV and a series of peaks through the high reflectivity region from the absorption edge through the visible and extending into the vacuum ultra-violet region. This data, of course, must be extrapolated into the unmeasured regions by the methods we have outlined in Section II, above. The remainder of this subsection details the extrapolation and other aspects of the method.

The data were analyzed as follows. It was found that a minimum of two sets of classical charge oscillators with different resonant frequencies was required in order to extrapolate the data consistently both at high frequencies and at low frequencies using (12) and (13). The criteria for good extrapolation that were employed were (a) the residual portion, i.e.,  $\Delta(\omega)$  in (11) should be as small as reasonably possible at the boundaries

# APPENDIX A

-12-

of the data, and (b)  $\Delta(\omega)$  should be rather smooth function. These criteria insure the applicability of the analysis in II above as well as good convergence of the Hermite expansion of  $\Delta(\omega)$ . For the reflectivity spectrum in Fig. 1 it was found that a good extrapolation was obtaining by choosing  $\hat{n}_0(\omega)$  from (12) as

$$\hat{n}_0 = 1 + \frac{20}{((2.5)^2 - \omega^2) + i(1)(\omega)} + \frac{90}{((11.8)^2 - \omega^2) + i(8.5)(\omega)} \quad (15)$$

Of course the function above is unit-free, however, the units of frequency in which it can be interpreted are electron volts. Hence we have used charged oscillator systems with resonant frequencies 2.5 and 11.8 eV.

Fig. 2 shows the function  $\Delta(\omega)$  which is obtaining by using for the  $g(\omega)$  of section II  $\ln \rho_0(\omega)$  as computed from (15) and subtracting that function from  $\ln r(\omega)$  obtained from the data. The contribution to the phase from  $\ln \rho_0(\omega)$  is obtained from (14).  $\Delta(\omega)$  has been expanded in a Hermite series to order 250 for which the expansion coefficients have been computed by Simpson's rule with the integrand evaluated at each 0.05 eV interval. Since the data extends to only 12.0 eV and the 250th Hermite function becomes essentially zero beyond the "classical turning point",  $\omega_{top} = \sqrt{501}$ , it is useful to scale in frequency in order to optimize the use of the higher order Hermite functions in the expansion. Thus the Hermite expansion coefficients of  $\Delta(\omega)$  are given by

$$\Delta_n(\alpha) = \int_{-\alpha\omega_{top}}^{\alpha\omega_{top}} \Delta_1(\alpha\omega) \phi_n(\alpha\omega) d(\alpha\omega) \quad (16)$$

where  $\Delta_1(\alpha\omega) = \Delta(\omega)$ .

## APPENDIX A

-13-

If  $\alpha = \sim 1.77$  we have found that the mean square error between  $\Delta(\omega)$  and its Hermite expansion is made minimal. The error function  $\chi(\omega)$  is plotted in Fig. 3 and in that figure  $\langle \chi^2(\omega) \rangle_{250}$  is given as  $4.54 \times 10^{-6}$ . Thus the expansion of  $\Delta(\omega)$  is accurate to an r.m.s. value of order  $10^{-3}$ . Since we know the matrix  $S_{nm}$  to be compact the convergent expansion of  $\phi(\omega)$  is easily computed from (6). The logarithm of the reflectivity amplitude and its phase,  $\phi(\omega)$ , are shown in Fig. 4 for  $\text{Sb}_2\text{Se}_3$ .

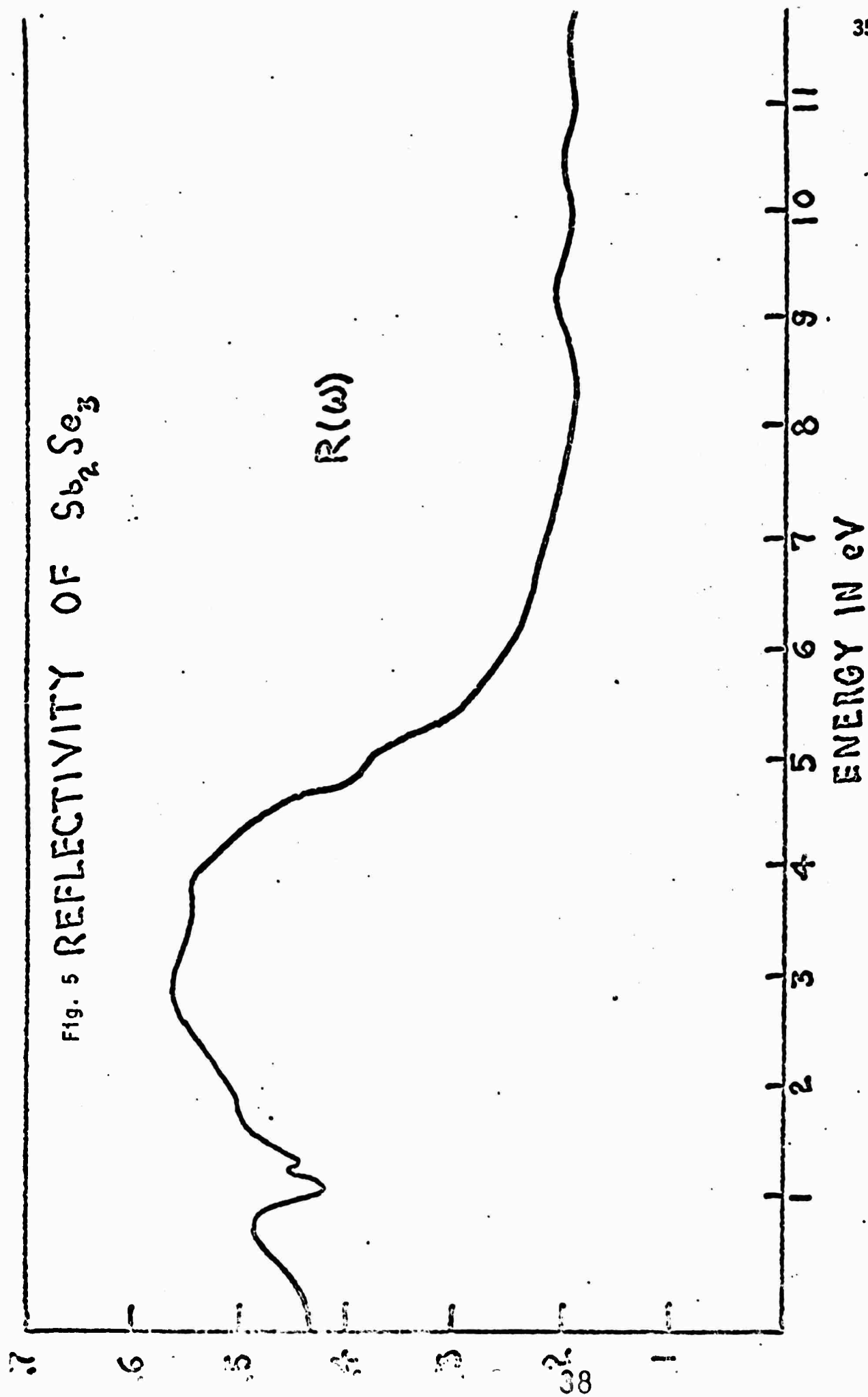
The Kramers-Kronig analysis is now complete and the optical functions of the system can easily be computed from (2) and related equations. Fig. 5 shows the real and imaginary parts of the index of refraction which we have obtained and Fig. 6 the real and imaginary parts of the complex dielectric function. It may be seen that the frequency positions of critical points are preserved through the transform process by comparing Figs. (5) and (6) with Fig. (1).

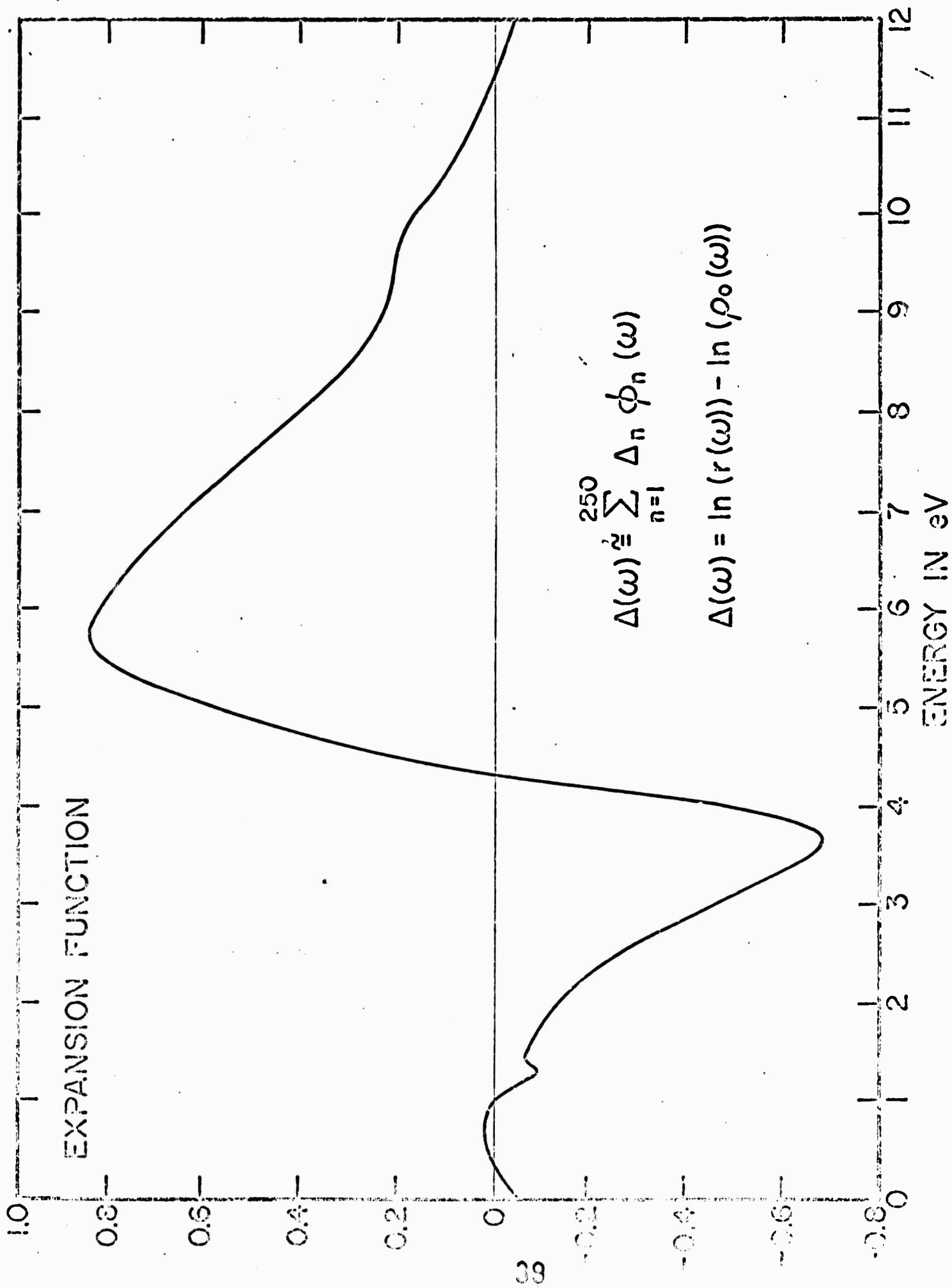
## APPENDIX A

### References

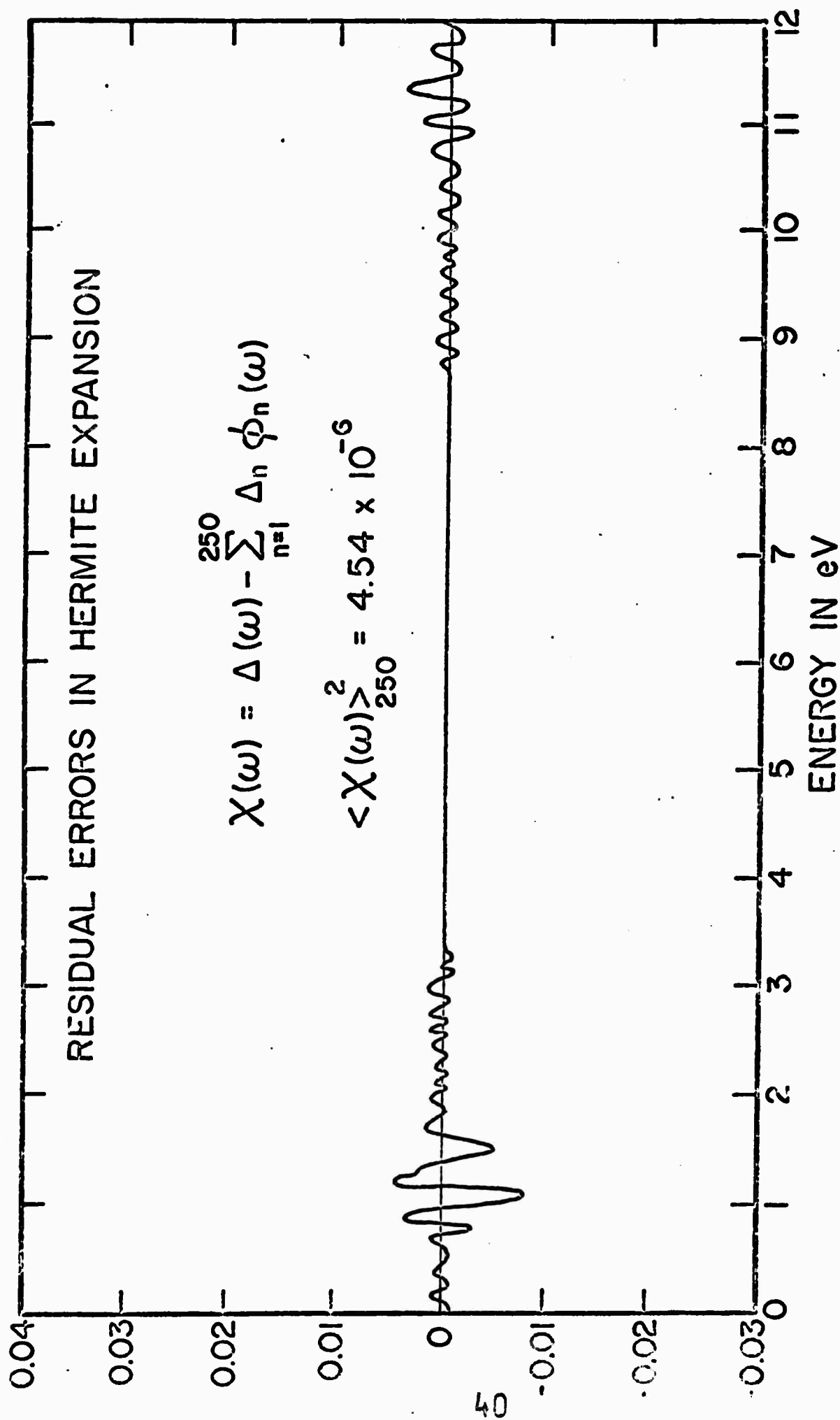
1. H. R. Phillipp and E. A. Taft, Phys. Rev. 113, 1002 (1959).
2. H. R. Phillipp and E. A. Taft, Phys. Rev. 136, A1445 (1964).
3. H. R. Phillipp and H. Ehrenreich, Phys. Rev. 129, 1550 (1963).
4. M. Cardona, Chap. VI, Optical Constants of Insulators, Ed. (Nudelman and Mitra), Plenum Press (1969).
5. Afshar, R., Mueller, F. M., and Shaffer, J. C. (submitted for publication).
6. Van Pelt, B., and Wood, C., Bull. Am. Phys. Soc., 16, 306 (1971).
7. Rubloff, G. W., Freeouf, J., Fritzche, H., and Morase, K., Phys. Rev. Ltrs., 26, 1317 (1971).
8. Page, C. H., Physical Mathematics, Van Nostrand (1955).
9. Shutov, S. D., Sobolev, V. V., Popov, Y. V., and Shestataskii, S. N., Phys. Stat. Sol. 31, K23, (1969).

Fig. 5 REFLECTIVITY OF  $Sb_2Se_3$









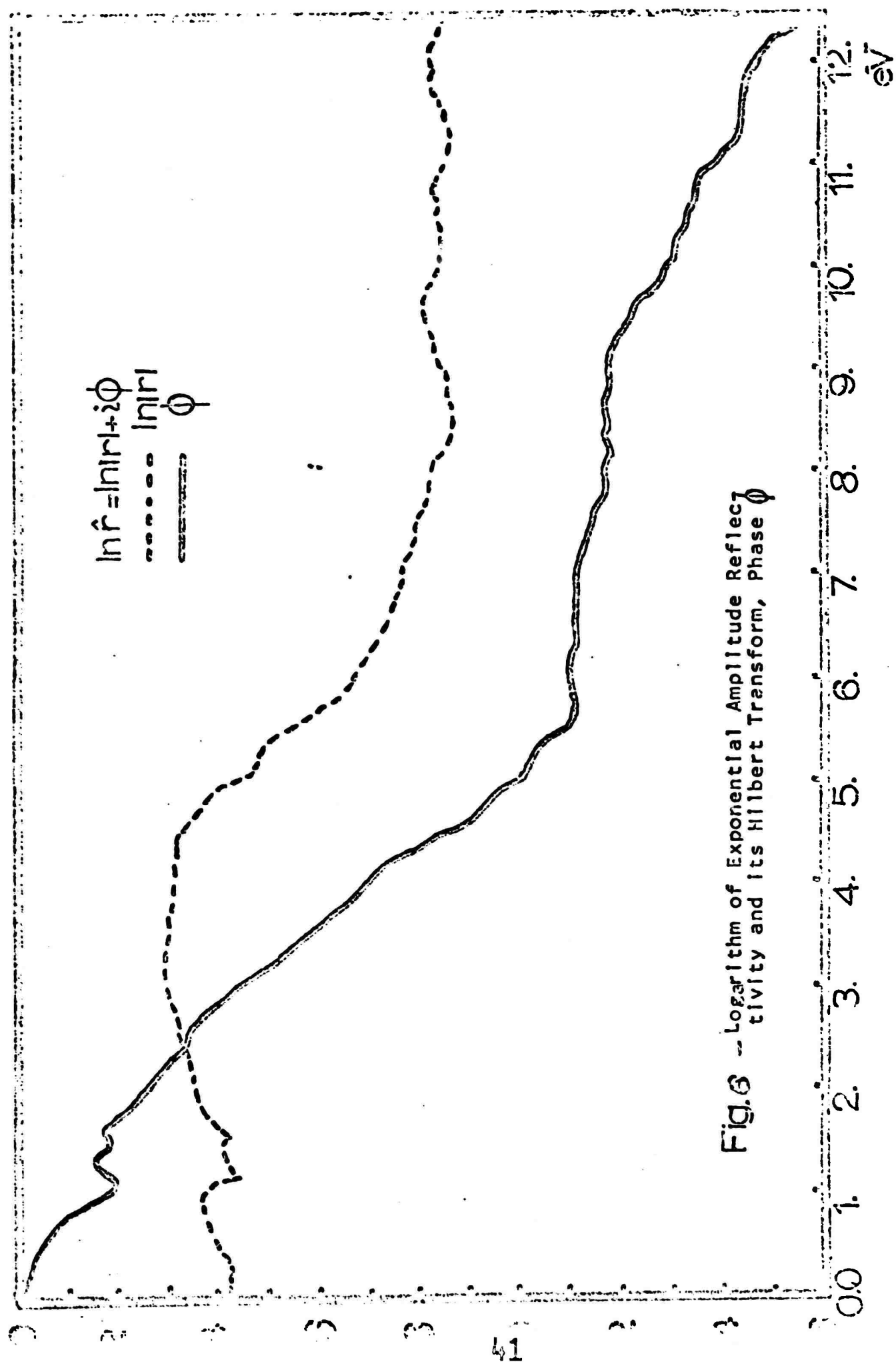
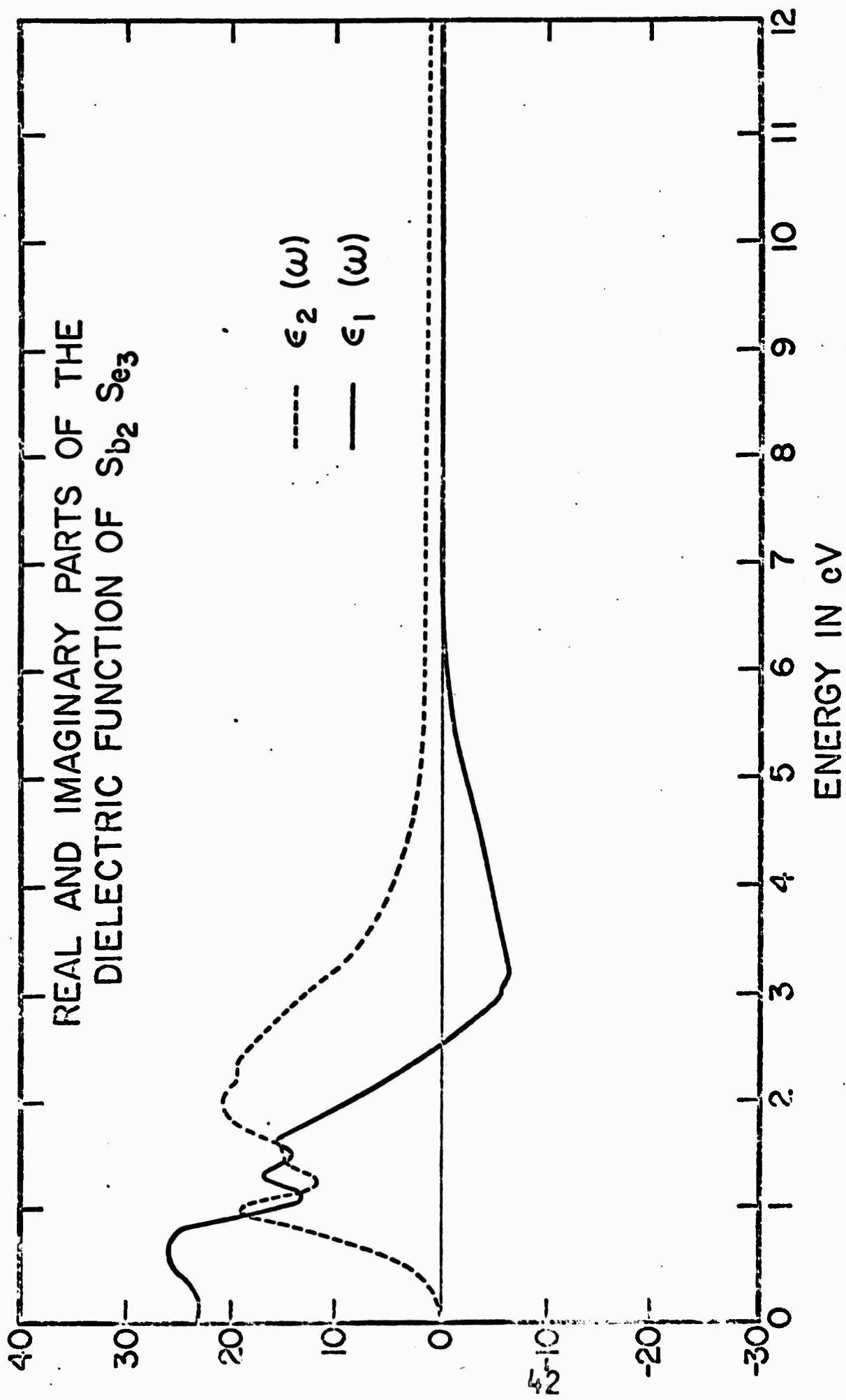
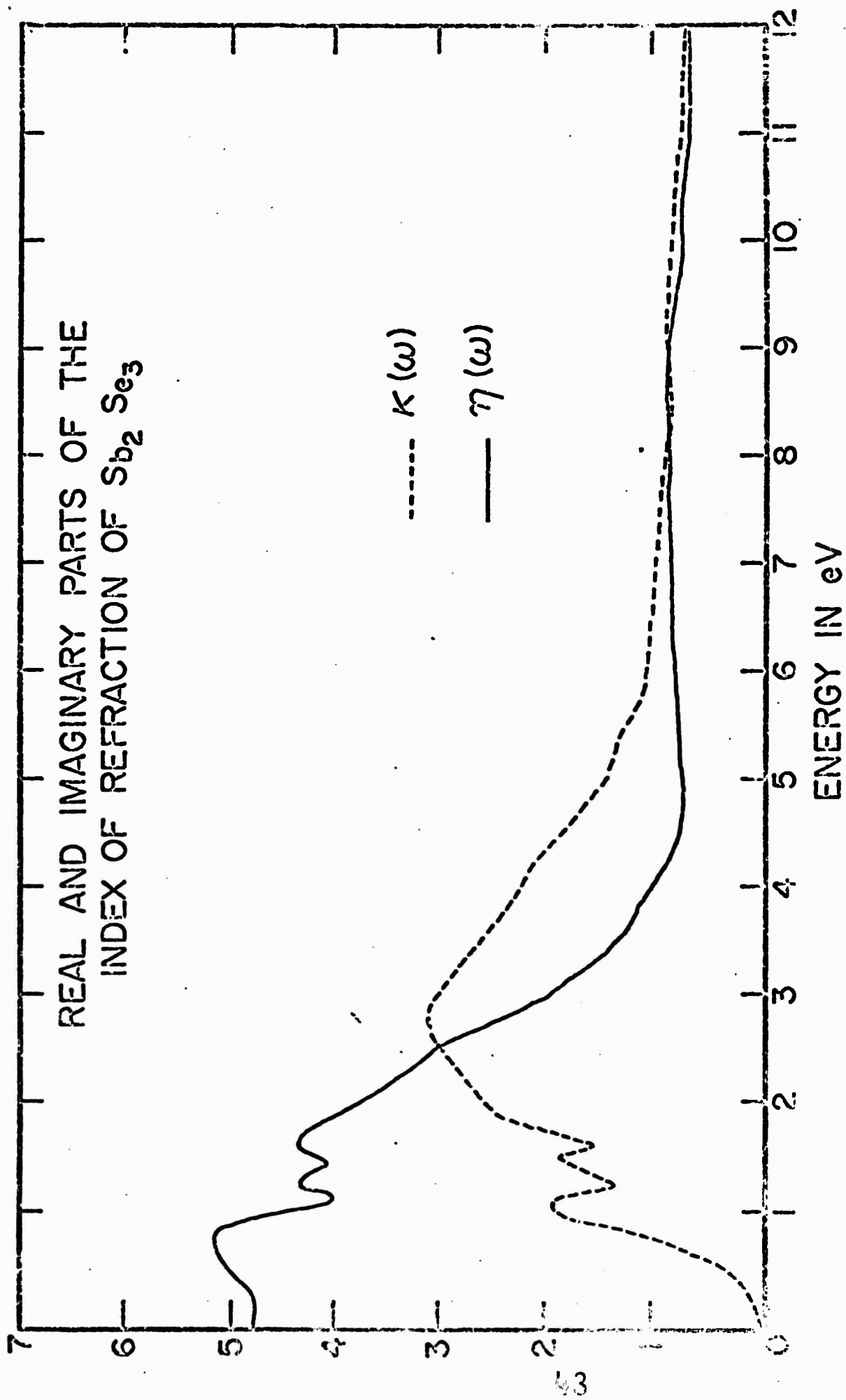


Fig. 6 -- Logarithm of Exponential Amplitude Reflectivity and its Hilbert Transform, Phase  $\phi$



REAL AND IMAGINARY PARTS OF THE  
INDEX OF REFRACTION OF  $\text{Sb}_2\text{Se}_3$



## APPENDIX B

## APPENDIX B

### Abstract Submitted

For the 1971 March Meeting of  
The American Physical Society

29 March - 1 April 1971  
Date

Physical Review  
Analytic Subject Index  
Number 44.4

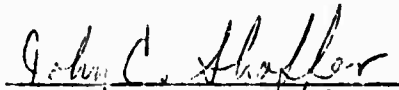
Bulletin Subject Heading in  
which Paper should be placed  
Optical Properties of Solids

The Optical Functions of Crystalline  $\text{Sb}_2\text{Se}_3$  from a Kramers-Krönig Analysis.\* J. C. SHAFFER and R. AFSHAR, Northern Illinois Univ.--In this contribution we present the results of a Kramers-Krönig analysis of normal incidence reflectivity data taken on  $\text{Sb}_2\text{Se}_3$  single crystals. The computational method<sup>1</sup> employed for the data analysis which is based upon expansion in Hermite functions and suitable high frequency extrapolations is presented as are the resulting optical functions. The accuracy and computational utility of the method and the relationship of the optical functions to the electronic structure of  $\text{Sb}_2\text{Se}_3$  are discussed.

\*Supported by A.R.P.A. through A.R.O., Durham.

<sup>1</sup>R. Afshar, F. M. Mueller, and J. C. Shaffer, (to be published).

Submitted by

  
Signature of APS Member

John C. Shaffer  
Same name typewritten

Department of Physics, NIU  
Address

DeKalb, Illinois 60115

## APPENDIX B

Abstract Submitted

For the 1971 March Meeting of

The American Physical Society

29 March - 1 April 1971

Date

Physical Review  
Analytic Subject Index  
Number 47.4

Bulletin Subject Heading in  
which Paper should be placed  
Semiconductors - Optical  
Properties

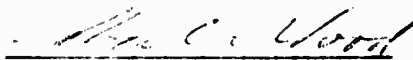
Optical Properties of Amorphous Antimony Selenides.\* C. WOOD, R. MUELLER, L.R. GILBERT, Z. HURYCH and C.C. WANG, Northern Illinois Univ.--Amorphous films of antimony selenides were prepared by the standard technique of vacuum evaporation from the compound  $\text{Sb}_2\text{Se}_3$ . Micro-probe analysis showed that the films deviate considerably from the stoichiometry the exact composition depending on the source temperature.<sup>1</sup> Evaporation from melts of  $\text{SbSe}_{0.9}$  yielded amorphous films of  $\text{Sb}_2\text{Se}_3$ . Amorphous films of various compositions were also prepared by controlled coevaporation of Sb and Se from separate sources. Optical transmission, reflectivity and photoconductivity measurements showed large changes in the forbidden energy gap as a function of composition. In contrast to many other amorphous materials and published data on antimony selenide films<sup>2</sup> the forbidden energy gaps of amorphous and single crystal  $\text{Sb}_2\text{Se}_3$  are approximately equal.

\*Supported by A.R.P.A. through A.R.O., Durham.

<sup>1</sup>A. Efsthion, D. M. Hoffman and E. R. Levin, J. Vacuum Sci. and Tech. 6, 383 (1969).

<sup>2</sup>B. T. Kolomiets, V. M. Lyubin and D. V. Tarkhin, Sov. Phys. Sol. State 1, 819 (1959).

Submitted by



Signature of APS Member

Charles Wood

Same Name typewritten

Department of Physics, NIU  
Address

DeKalb, Illinois 60115

## APPENDIX B

Abstract Submitted

For the 1971 March Meeting of  
The American Physical Society

29 March - 1 April 1971  
Date

Physical Review  
Analytic Subject Index  
Number 48.3

Bulletin Subject Heading in  
which Paper should be placed  
Amorphous Solids

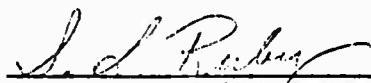
Mossbauer Studies on Amorphous and Crystalline Antimony Selenides.\* S.L. RUBY, Argonne National Lab., L.R. GILBERT and C. WOOD, Northern Illinois Univ.--Mossbauer resonance spectra at 4°K were determined for a range of compositions of amorphous  $\text{SbSe}_x$ , where  $0.5 < x < 9$ , and compared with the spectrum of crystalline  $\text{Sb}_2\text{Se}_3$ . The amorphous compositions were thick films prepared by vacuum evaporation and were determined to be amorphous by X-ray diffraction. The composition was determined by X-ray emission spectroscopy. A double peak was observed in the Mossbauer spectrum of crystalline  $\text{Sb}_2\text{Se}_3$  which could be fitted by postulating two equally populated sites for the Sb atoms in agreement with X-ray data.<sup>1</sup> In all compositions of amorphous  $\text{SbSe}_x$  only a single peak was obtained which was located at an intermediate position between the double peaks in the crystalline material. These results show that the short range order in amorphous  $\text{SbSe}_x$  differs from the crystalline solid, thus supporting the conclusions of Tatarinova<sup>2</sup> from electron diffraction studies.

\*Partially supported by A.R.P.A. through A.R.O., Durham.

<sup>1</sup>N.W. Tideswell, F.H. Kruse, and J.D. McCullough, Acta Cryst. 10, 99 (1957).

<sup>2</sup>L.I. Tatarinova, Kristallografiya 4, No. 5, 678 (1959).

Submitted by

  
Signature of APS Member

S. L. Ruby  
Same name typewritten

Argonne National Lab.  
Address

Argonne, Illinois 60439



## APPENDIX B

### Abstract Submitted

For the 1971 March Meeting of  
The American Physical Society

29 March - 1 April 1971  
Date

Physical Review  
Analytic Subject Index  
Number 48.3

Bulletin Subject Heading in  
which Paper should be placed  
Amorphous Solids

Mossbauer Investigation of  $\text{Sn}_x(\text{As}_2\text{Se}_3)_{1-x}$   
Glasses.\* S.P. TANEJA, L. GILBERT, W.C. HARPER, C.W.  
KIMBALL, and C. WOOD, Northern Illinois Univ.--The depen-  
dence of conductivity and microhardness of glasses of the  
Sn-Se-As system has been attributed by Shkol'nikov<sup>1</sup> to a  
transition from  $\text{SnSe}_2$  to  $\text{SnSe}$  with increasing tin concen-  
tration. However, Borisova et al<sup>2</sup> infer that  $\text{SnSe}_2$  is  
found only in the glassy state and  $\text{SnSe}$  only in the crys-  
talline state. In the present investigation of glasses  
of  $\text{Sn}_x(\text{As}_2\text{Se}_3)_{1-x}$  (with  $x = 2.5, 5.0, 8.0, 10.0$  atomic per-  
cent) were prepared by quenching the melts into a brine  
bath at  $\sim 200^\circ\text{K}$ . X-ray patterns show distributions char-  
acteristic of a glass; further, the patterns are qualita-  
tively similar for all compositions. The Mossbauer study  
confirms the  $\text{SnSe}_2$ - $\text{SnSe}$  transition with increasing tin  
concentration.<sup>1</sup> The line width and concentration depen-  
dence of the isomer shift indicate a high degree of  
local order. The question of the presence of micro-  
crystallinity will be discussed.

\*Work supported by A.R.P.A. through A.R.O., Durham.

<sup>1</sup>E. V. Shkol'nikov, Solid State Chemistry ed. Z. N.  
Borisova (Consultants Bureau, N.Y. 1966) p. 142.

<sup>2</sup>Z. U. Borisova et al, Sov. Phys. - Semiconductors 4,  
443 (1970).

Submitted by

Clyde W. Kimball  
Signature of APS Member

Clyde W. Kimball  
Same name typewritten

Physics Department, NIU  
Address

DeKalb, Illinois 60115

## APPENDIX B

### Abstract Submitted

For the 1971 March Meeting of  
The American Physical Society

29 March - 1 April 1971  
Date

Physical Review  
Analytic Subject Index  
Number 47.4

Bulletin Subject Heading in  
which Paper should be placed  
Semiconductors - Optical  
Properties

Optical Properties of  $\text{Sb}_2\text{Se}_3$  Single Crystals.\*  
B. VAN PELT and C. WOOD, Northern Illinois Univ.--The  
optical absorption and transmission of single crystal  
 $\text{Sb}_2\text{Se}_3$  has been measured in the region of the absorp-  
tion edge with respect to the principal crystallogra-  
phic axes. The optical transitions responsible for  
the edge will be discussed.

\*Supported by A.R.P.A. through Army Research Office,  
Durham.

Submitted by



Signature of APS member

Charles Wood  
Same name typewritten

Department of Physics, NIU  
Address

DeKalb, Illinois 60115

Please place this paper together with and preceeding the  
accompanying paper Photoconductivity in Single Crystals  
of  $\text{Sb}_2\text{Se}_3$  by Z. Hurych, et al.

## APPENDIX B

Abstract Submitted

For the 1971 March Meeting of

The American Physical Society

29 March - 1 April 1971

Date

Physical Review  
Analytic Subject Index  
Number 47.5

Bulletin Subject Heading in  
which Paper should be placed  
Semiconductors - Transport  
Properties

### Photoconductivity in Single Crystals of $\text{Sb}_2\text{Se}_3$ .\*

Z. HURYCH, C.C. WANG and C. WOOD, Northern Illinois Univ.—The activation energy  $\Delta E_a$ , the response time  $\tau$  and the spectral distribution of photocurrent  $I_{ph}$  were measured for p-type semiconducting orthorhombic single crystals of  $\text{Sb}_2\text{Se}_3$  as a function of the orientation of the electric vector  $E_0$  of the polarized light and of the drift field  $E_d$  with respect to the three crystallographic axes, a, b, and c. Values of  $\Delta E_a$  were 1.09, 1.10 and 1.13 eV for  $E_0 \parallel a$ , b, and c, respectively, in good agreement with corresponding optical activation energies and with published data on photoconductivity using nonpolarized light.<sup>1</sup> Values of  $\tau$  were in the region 300–400  $\mu$  sec for  $h\nu = 1.1$  eV, and indicate presence of trapping levels inside the forbidden gap. The spectral distribution of  $\tau$  and  $I_{ph}$  as a function of  $E_0$  and  $E_d$  orientations will be discussed.

\*Supported by A.R.P.A. through A.R.O., Durham.

<sup>1</sup>B. T. Kolomiets and A. Kh. Zeinaly, Sov. Phys. Sol. State 1, 896 (1959).

Submitted by

  
Signature of APS member

Charles Wood  
Same name typewritten

Department of Physics, NIU  
Address

DeKalb, Illinois 60115

Please place this paper together with and following the accompanying paper Optical Properties of  $\text{Sb}_2\text{Se}_3$  Single Crystals by B. Van Pelt and C. Wood.

**APPENDIX C**

## APPENDIX C

Abstract Submitted

For the 1971 April Meeting of  
The American Physical Society

26 April - 29 April 1971  
Date

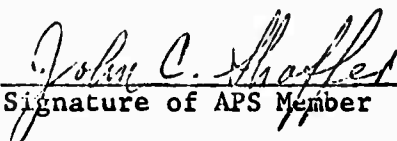
Physical Review  
Analytic Subject Index  
Number 44.4

Bulletin Subject Heading in  
which Paper should be placed  
Optical Properties of Solids

The Optical Constants of Thin Amorphous Films of  
Sb<sub>x</sub>Se<sub>y</sub>.\* J.C. SHAFFER, R. AFSHAR, C. WOOD, and R. MUE-  
LER, Northern Illinois Univ.--The optical functions of  
thin films are often difficult to obtain due to compli-  
cations arising from the occurrence of interference in  
their reflection and transmission spectra. We present  
and discuss an experimental and computational method for  
circumventing this problem. We obtain from reflectance  
measurements via Kramers-Kronig analysis the optical  
functions of films, sufficiently thick ( $>5\mu$ ) that inter-  
ference effects are largely suppressed. These optical  
functions are employed to compute exactly the reflect-  
ance and transmittance for thinner ( $\sim 1,000\text{\AA}$ ) films with  
identical optical functions. The results are compared  
with experimental reflectance and transmission of  
thinner films of the same composition. These films are  
prepared simultaneously with the thick films by co-evap-  
oration. The method is applied to amorphous films of  
Sb<sub>x</sub>Se<sub>y</sub> and comparison made with the optical functions of  
crystalline Sb<sub>2</sub>Se<sub>3</sub>.

\*Supported by A.R.P.A. through Army Research Office,  
Durham.

Submitted by

  
Signature of APS Member

John C. Shaffer  
Same name typewritten

Physics Department, NTU  
Address

DeKalb, Illinois 60115

## APPENDIX C

Abstract Submitted

For the 1971 April Meeting of  
The American Physical Society

26 April - 29 April 1971  
Date

Physical Review  
Analytic Subject Index  
Number 48.3

Bulletin Subject Heading in  
which Paper should be placed  
Amorphous Solids

Glass-Crystalline Transitions in Amorphous  
Sb<sub>x</sub>Se<sub>y</sub>. \* L.R. GILBERT and C. WOOD, Northern Illinois Univ.  
The glass transition temperature in amorphous antimony  
selenides shows a strong dependence on composition. At  
the composition Sb<sub>2</sub>Se<sub>3</sub> the transition occurs at ~180-200°C  
in agreement with the nucleation studies of Bolotov et al.  
The transition temperatures were determined by differen-  
tial thermal analysis and resistivity versus temperature  
measurements and are compared.

\*Supported by A.R.P.A. through A.R.O., Durham.

<sup>1</sup>I.E. Bolotov, A.V. Kozhin, and S.B. Fishelova, Sov.  
Phys.-Cryst. 15, 461 (1970).

Submitted by



Signature of APS Member

Charles Wood

Same name typewritten

Physics Department, NIU  
Address

DeKalb, Illinois 60115

APPENDIX C

Abstract Submitted

For the 1971 April Meeting of  
The American Physical Society

26 April - 29 April 1971  
Date

Physical Review  
Analytic Subject Index  
Number 47.4


Bulletin Subject Heading in  
which Paper should be placed  
Semiconductors - Optical  
Properties

Thermally Modulated Reflectivity of  $\text{Sb}_2\text{Te}_3$ .\*  
C. WOOD, Z. HURYCH, and B. VAN PELT, Northern Illinois  
Univ.--The thermally modulated reflectivity has been  
determined in the visible and near IR region of the  
spectrum for single crystals of  $\text{Sb}_2\text{Te}_3$  with the electric  
vector of the radiation in the cleavage plane ( $E \parallel C$ ). The  
data show the same critical points as observed in the  
optical transmission spectrum of very thin cleaved speci-  
mens using a photon counter. These results are compared  
with the low temperature reflectivity data of Sobolev  
et al.<sup>1</sup>

\*Supported by A.R.P.A. through A.R.O., Durham.

<sup>1</sup>V.V. Sobolev, S.D. Shutov, Yu. V. Popov, and S.N.  
Shestatskii, phys. stat. sol. 30, 349 (1968).

Submitted by

  
Signature of APS Member

Charles Wood  
Same name typewritten

Physics Department, NIU  
Address

DeKalb, Illinois 60115

APPENDIX D



## APPENDIX D

### MOSSBAUER STUDIES ON AMORPHOUS AND CRYSTALLINE ANTIMONY SELENIDES

S. L. Ruby  
Physics Division  
Argonne, Illinois

and

L. R. Gilbert\* and C. Wood\*  
Physics Department  
Northern Illinois University  
DeKalb, Illinois 60115

Mossbauer resonance spectra at 4<sup>0</sup>K have been determined for a range of compositions of amorphous SbSe<sub>x</sub> films, where 0.5 < x < 9, and were compared with the spectrum of crystalline Sb<sub>2</sub>Se<sub>3</sub>. The crystal structure of Sb<sub>2</sub>Se<sub>3</sub> is orthorhombic Pbnm ( $D_{2h}^{16}$ )<sup>5</sup> consisting of infinite chains parallel to the c-axis. There are two different equally populated Sb sites and three different Se sites within the crystal lattice. The strongest bonds are within the chains and here the Sb-Se bond distances range from 2.576<sup>0</sup>Å to 2.777<sup>0</sup>Å, while the 'non-bonded' Sb-Se separations range from 2.98<sup>0</sup>Å to 3.74<sup>0</sup>Å<sup>1</sup>.

The Mossbauer spectrum of a powdered sample of crystalline Sb<sub>2</sub>Se<sub>3</sub> is shown twice in Fig. 1. The solid line in the upper curve is the (unsuccessful) result of a computer fit assuming a single Sb lattice site. In the lower fit, the computer was allowed two different, but equally populated Sb sites. Now  $\chi^2$  shrinks to 1.2 versus 7.3 in the

---

\* This research was supported by the Advanced Research Projects Agency of the Department of Defense and was monitored by the Army Research Office, Durham, under Contract No. DA-ARO-D-31-127-70-G77.

## APPENDIX D

summarize, it seems that for a best fit a range in  $e^2qQ$  and  $S_I$  are required averaging near the values given above.

The above results show that the short range order in amorphous  $SbSe_x$  differs from that of the crystalline solid, and indicates a close conformity in the environment, i.e., a narrow range of coordination number and Sb-Se bond lengths, of each Sb atom in the amorphous solid. Electron diffraction studies of Tatarinova<sup>2</sup> lend support to this viewpoint. Intensity and radial distribution curves indicate that both the coordination number and nearest neighbor distances decrease in the transition from the crystalline to the amorphous phase of " $Sb_2Se_3$ ". (The composition may have been Se-rich from the method of preparation described in the article). In contrast,  $As_2Se_3$  and GaAs were shown to retain in the amorphous phase the configuration inherent in the crystalline phase.

The above results resemble those from previous Mossbauer studies on glassy materials in which  $Fe_2O_3$  was dissolved in both silicate and phosphate glasses<sup>3</sup>. The microenvironments of the  $Fe^{3+}$  ion in each case were found to be similar although the coordination was tetrahedral in the silicate and octahedral in the phosphate glass. Despite the glassy nature of the material in these cases, as well as in the antimony work done here, there does not seem to be a wide variety of microenvironments. However, in the amorphous  $Sb-Se_x$  films, we have a different microenvironment than in the crystalline material.

These results are of significance to questions of whether a vapor-quenched solid is truly a glass or consists of micro-crystals; particularly

## APPENDIX D

upper fit. The Mossbauer isomer shifts for the two peaks were 12.6 mm/sec and 15.5 mm/sec.

The amorphous thick ( $\sim 30$  microns) films were prepared by vacuum evaporation onto room-temperature quartz substrates from large sources of various ratios of Sb and Se. The films were determined to be amorphous by x-ray diffraction. The composition as deposited (invariably different from the source material) was determined by electron microprobe and/or x-ray emission spectroscopy. For example, a source at a temperature of  $720^{\circ}\text{C}$  with  $x = 1.5$  (i.e.,  $\text{Sb}_2\text{Se}_3$ ) produced a film with  $x \sim 9$ . Amorphous films of various compositions in the range  $0.5 < x < 9$  were prepared and measured and the results are shown in Table 1. In all compositions of amorphous  $\text{SbSe}_x$  only a single peak was obtained which was located at an intermediate position between the double peaks in the crystalline material, as illustrated in Fig. 2.

In  $^{121}\text{Sb}$  Mossbauer spectroscopy, working between nuclear levels with spins of  $7/2$  and  $5/2$ , a pure quadrupole interaction gives rise to an asymmetric octet. In the present case, the quadrupole interaction is not large enough compared to the minimum line width of 7.1 mm/sec to resolve these individual lines. It is found (see Fig. 1) that the data for the amorphous films can be moderately well fitted by a single site where each member of the octet has a normal width  $\Gamma = 2.8$  mm/sec, the value of  $e^2qQ$  is  $10.5 \pm 1$  mm/sec and the isomer shift is  $-13.5 \pm 0.5$  mm/sec. By adding more freedom to the computer program (allowing more sites),  $\chi^2$  can be further decreased. To

## APPENDIX D

in systems where the glass cannot be readily formed from a melt-quench, as in the case of  $\text{Sb}_2\text{Se}_3$ . We can state that if the film is an assemblage of microcrystals, the crystal structure does not correspond to the equilibrium phase and the more probable conclusion is that it is amorphous. The occurrence of a softening temperature ( $T_g$ ) in the films would support this conclusion.

The authors wish to thank Dr. Kimball for many helpful discussions.

## REFERENCES

1. N. W. Tideswell, F. H. Kruse and J. C. McCullough, *Acta Cryst.* 10, 99 (1957).
2. L. I. Tatarinova, *Kristallografiya* 4, No. 5, 678 (1959).
3. C. R. Kurkjian and E. A. Sigety, *Phys. Chem. Glasses*, 9, 3 (1968).

# APPENDIX D

## TABLE 1

$\text{SbSe}_x$	Phase	$x^2$	$S_I$	$e^2qQ$	$\beta$
$x = 6.3$	Amorphous	.374	-13.97	9.64	3.39
4.4	Amorphous	.575	-14.42	9.70	2.68
2.0	Amorphous	.531	-113.38	10.85	3.26
1.5	Amorphous	1.206	-13.65	10.90	3.04
1.5	Cryst.	.253	-12.60	7.86	2.48
			-15.50	8.40	2.49
0.5	Amorphous	.466	-13.00	11.50	2.58

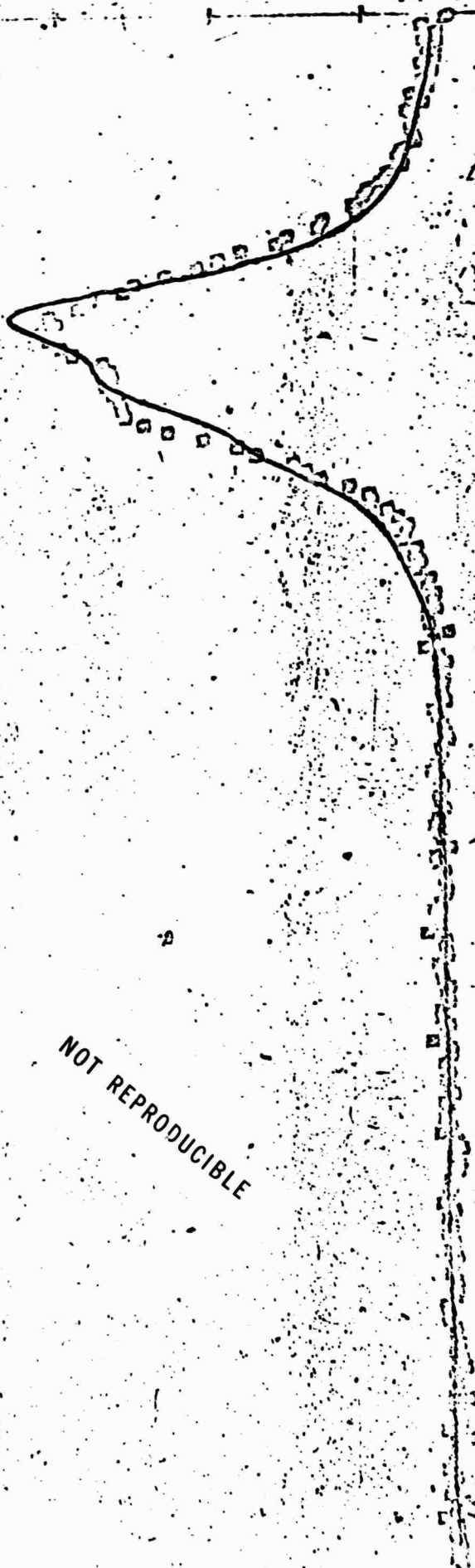
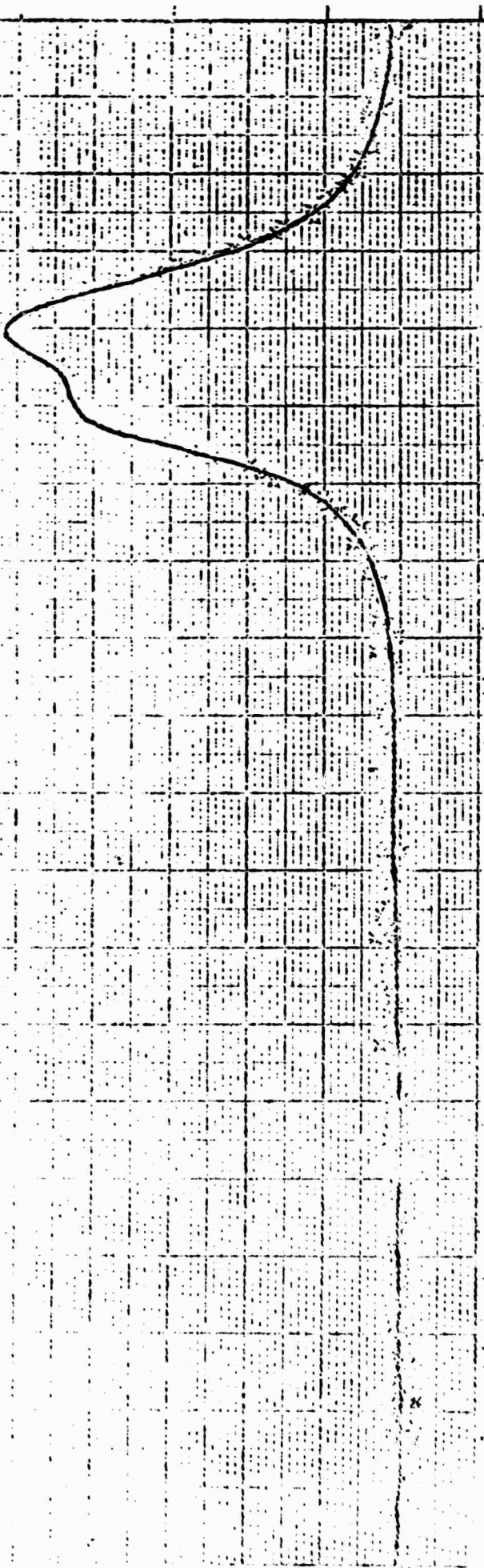
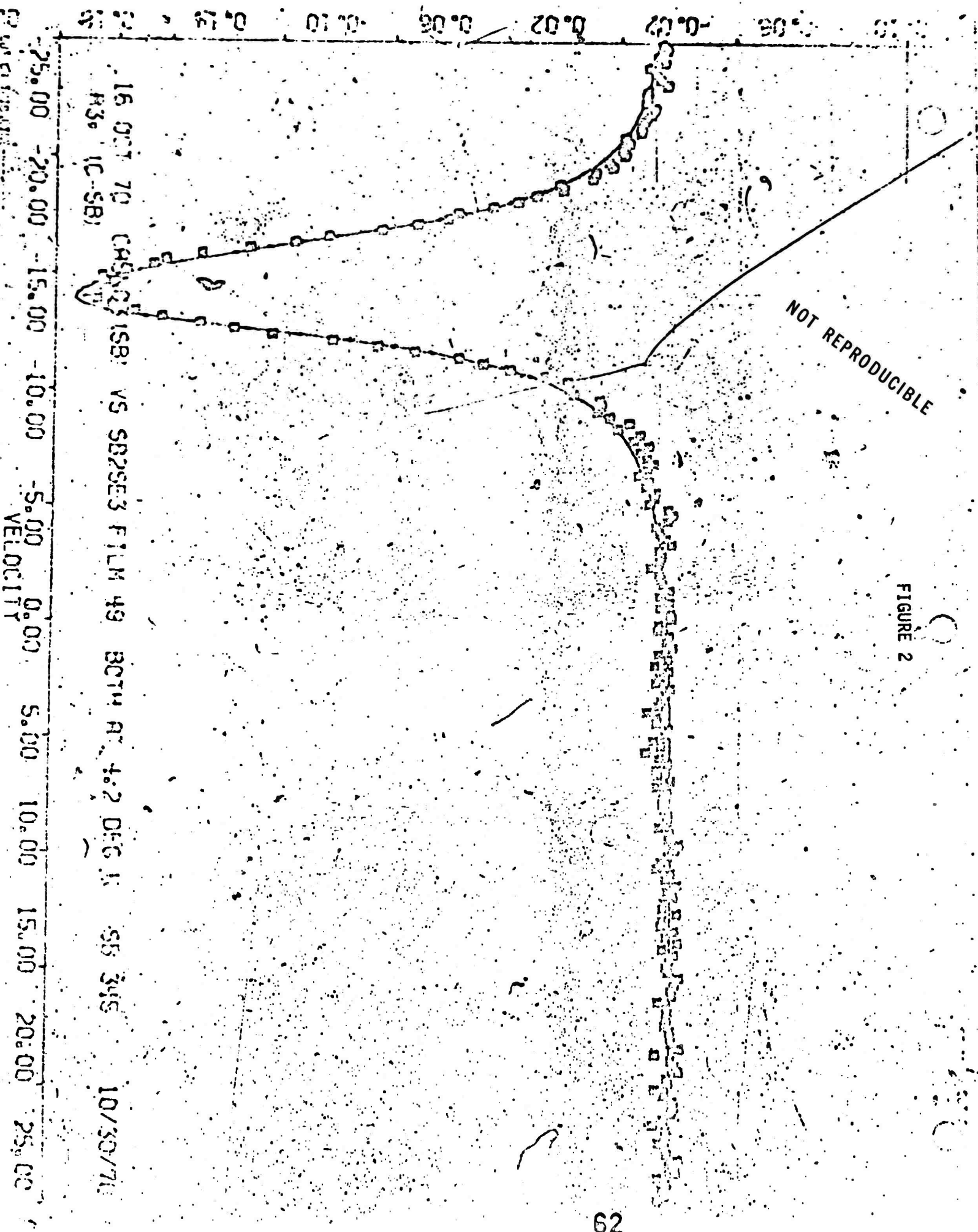


FIGURE 1

NOT REPRODUCIBLE



The Optical Properties of  $\text{Sb}_2\text{Se}_3$ - $\text{Sb}_2\text{Te}_3$ <sup>1)</sup>

By

W. PROCARIONE<sup>2)</sup> and C. WOOD

The optical properties of single crystal specimens of  $\text{Sb}_2\text{Te}_3$ - $\text{Sb}_2\text{Se}_3$  solid solutions have been investigated in the photon energy range 0.04 eV to 6.5 eV. A wide range of solid solutions having hexagonal structure were found to exhibit properties closely corresponding to the isostructural compounds  $\text{Bi}_2\text{Te}_3$  and  $\text{Bi}_2\text{Se}_3$ . Small indirect band gaps approaching semimetallic values were obtained. The high free-carrier concentrations gave rise to plasma effects in the near infra-red. In contrast  $\text{Sb}_2\text{Se}_3$  is orthorhombic with a direct band gap near 1 eV. The chemical bonding concepts applied to similar systems seem applicable with only slight modification.

Die optischen Eigenschaften von  $\text{Sb}_2\text{Te}_3$ - $\text{Sb}_2\text{Se}_3$ -Mischkristallen wurden im Bereich von 0,04 eV bis 6,5 eV untersucht. Die Festkörperlösungen haben innerhalb weiter Grenzen die gleiche hexagonale Struktur wie die isostrukturellen Verbindungen  $\text{Bi}_2\text{Te}_3$  und  $\text{Bi}_2\text{Se}_3$  und zeigen sehr verwandte optische Eigenschaften. Kleine indirekte Energieschwellen ähnlich denen in Halbleitern wurden beobachtet. Die große Konzentration von freien Ladungsträgern verursachte Plasmaerscheinungen im nahen Ultrarot.  $\text{Sb}_2\text{Se}_3$  ist orthorhombisch mit einem direkten verbotenen Energieband von 1 eV. Die chemischen Bindungskonzepte können wahrscheinlich mit nur geringen Veränderungen auf ähnliche Systeme angewendet werden.

## 1. Introduction

Binary compounds of the form  $\text{A}_2\text{BY}_3$  have been studied extensively in the past. Solid solutions of these compounds, particularly the isostructural systems of  $\text{Bi}_2\text{Te}_3$ - $\text{Bi}_2\text{Se}_3$  and  $\text{Bi}_2\text{Te}_3$ - $\text{Sb}_2\text{Te}_3$ , have received considerable attention in the literature. A few serious attempts have been made to study the detailed band structure of these compounds and their solid solutions; noteworthy among these being the optical work of Greenaway and Harbeke [1] on  $\text{Bi}_2\text{Te}_3$ - $\text{Bi}_2\text{Se}_3$ , and Sobolev et al. [2, 3], on  $\text{Bi}_2\text{Te}_3$ ,  $\text{Bi}_2\text{Se}_3$ , and  $\text{Sb}_2\text{Te}_3$ .

Except for some thermoelectric data by Teramoto and Takayanagi [4], the information on the physical properties of solid solutions of  $\text{Sb}_2\text{Te}_3$  and  $\text{Sb}_2\text{Se}_3$  appears to be almost non-existent. However, solid solutions of these two compounds represent an interesting system to study. Although possessing different crystallographic structures,  $\text{Sb}_2\text{Se}_3$  is orthorhombic ( $D_{2h}^{16}$ ) and  $\text{Sb}_2\text{Te}_3$  is rhombohedral ( $C_{3v}$ ) or hexagonal on a larger unit cell, a considerable range of solid solubilities exist in this system. X-ray analysis by Teramoto and Takayanagi [4] revealed that a single-phase hexagonal structure exists between  $\text{Sb}_2\text{Te}_3$  and  $\text{Sb}_2\text{TeSe}_2$  with the lattice constant,  $a$ , decreasing approximately from 4.27 Å to 4.12 Å and the lattice constant,  $c$ , decreasing approximately from 30.4 Å to 29.5 Å with increasing  $\text{Sb}_2\text{Se}_3$  content. Higher concentrations of  $\text{Sb}_2\text{Se}_3$  resulted in an admixture of hexagonal and orthorhombic phase.

<sup>1)</sup> Partially supported by A.R.P.A. through the Army Research Office, Durham.

<sup>2)</sup> This work partially fulfilled the requirements for the M.S. Degree in Physics.



As a start toward understanding the physical properties of this system, and obtaining a knowledge of the band structure, reflection and transmission measurements on single crystals in the range 0.04 eV to 6.5 eV were investigated. Because of the marked directional preference in cleavage, (0001) for hexagonal and (010) for orthorhombic crystals, and the difficulty of preparing good reflecting surfaces perpendicular to the cleavage planes, optical measurements have been made only with the electric vector in the cleavage plane.

Comparison of this data with the results of Greenaway and Harbeke [1] on  $\text{Bi}_2\text{Te}_3$ - $\text{Bi}_2\text{Se}_3$ , and Shutov et al. [3] on the end components,  $\text{Sb}_2\text{Te}_3$  and  $\text{Sb}_2\text{Se}_3$ , has shown many similarities between these systems but has raised questions concerning the chemical bonding concepts formulated to explain the properties of this class of materials.

## 2. Experimental Procedures

### 2.1 Preparation of materials

All starting materials were of six 9's purity. The antimony and tellurium were obtained from COMINCO, the selenium from Norddeutsche Raffinerie. Further purification was carried out on those elements used for preparing the end components of the system,  $\text{Sb}_2\text{Te}_3$  and  $\text{Sb}_2\text{Se}_3$ . For these, the antimony and tellurium were outgassed and sealed-off under a vacuum, and then zone-refined in a carbon crucible. The selenium was outgassed and sublimed under vacuo.

Single crystals or large grain size ingots were grown by the Bridgman technique or by a horizontal zone-refiner with background heating, described elsewhere [5]. Specimens for optical measurements were cleaved from these ingots down to a thickness of a few tens of microns by peeling a layer from the surface using Scotch-tape, or by mounting a thick specimen with epoxy onto an aluminum plate possessing a small aperture and then pulling the bulk of the material off the plate, leaving a thin layer behind.

Chemical analyses were performed on sections of these ingots to test for uniformity of composition and approximate correspondence with the nominal composition was obtained.

### 2.2 Optical measurements

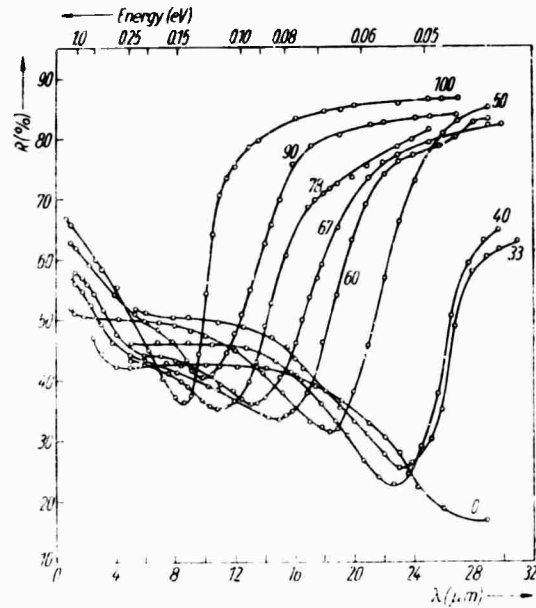
Transmission and reflectivity measurements in the energy range 6.5 eV to 2.0 eV (wavelength 0.18  $\mu\text{m}$  to 2.6  $\mu\text{m}$ ) were performed in a Cary double-beam 14R spectrophotometer. A Cary attachment, based on a V-W configuration by Strong [6] was used to measure reflectivity at near normal ( $< 12^\circ$ ) incidence, using an aluminum mirror as a standard reference. This attachment requires two reflecting samples.

A Beckman IR 12 spectrophotometer was used for transmission and reflectivity measurements in the range 2.0 eV to 0.04 eV (2.5  $\mu\text{m}$  to 35  $\mu\text{m}$ ). A standard Beckman attachment was used to measure reflectivity at an angle of incidence of  $\approx 28^\circ$ . A long wavelength limit of 35  $\mu\text{m}$  was imposed on the reflectivity measurements by the  $\text{CaBr}_2$  lenses in the attachment.

## 3. Reflectivity

The room-temperature reflectances ( $R$ ) of the  $\text{Sb}_2\text{Te}_3$ - $\text{Sb}_2\text{Se}_3$  solid solutions in the range 0.04 eV to 2.0 eV are shown in Fig. 1. The pronounced minima appear to be associated with the charge carrier plasma frequency; in this case,

Fig. 1. The long-wavelength reflectance spectra of  $\text{Sb}_2\text{Te}_3\text{-Sb}_2\text{Se}_3$  solid solutions. The numbers refer to at%  $\text{Sb}_2\text{Te}_3$ .



a hole plasma, since all materials were determined to be p-type by sign of the Seebeck coefficient. A calculation of the approximate position of  $\omega_p$ , the plasma frequency minimum [7] for  $\text{Sb}_2\text{Te}_3$  from

$$\omega_p^2 = \frac{p e^2}{m^* \epsilon_0 (n_c^2 - 1)} = \frac{\sigma e}{m^* \mu \epsilon_0 (n_c^2 - 1)} \quad (1)$$

where  $p$  charge carrier concentration,  $e$  electronic charge,  $m^*$  effective mass,  $\epsilon_0$  permittivity of free space,  $\sigma$  conductivity,  $\mu$  mobility, and  $n_c$  the refractive index in the non-dispersive region of the spectrum, using values<sup>3)</sup> of  $p$ ,  $m^*$ , and  $n_c$  from Testardi et al. [8] gave a value of 7  $\mu\text{m}$  which is in reasonable agreement with experiment. Furthermore, the plasma frequency minima for  $\text{Sb}_2\text{Te}_3$  samples, doped with various amounts of copper, shift with the square root of conductivity giving additional confirmation of this assignment.

The minima for the  $\text{Sb}_2\text{Te}_3\text{-Sb}_2\text{Se}_3$  solid solutions move toward longer wavelengths with increasing amounts of  $\text{Sb}_2\text{Se}_3$ . Again, the shift in position correlates surprisingly well with the square root of the conductivity considering no allowance was made for mobility variations.

In Fig. 2 the reflectance values at higher energies are shown and pronounced maxima are observed in the range 1 eV to 6 eV. By analogy with  $\text{Bi}_2\text{Te}_3$ , these maxima are probably due to direct interband transitions which should be associated with critical points at or between the  $\Gamma(000)$  and  $Z(111)$  points of the Brillouin zone [1]. If this band model is correct, then any fine structure in the curves would be due to a spin orbit split valence band. However, this model

<sup>3)</sup> Published values by various investigators of  $p$  (and  $\sigma$ ) for undoped  $\text{Sb}_2\text{Te}_3$  are in close agreement. The approximate value of  $n_c$  is obtained from the curve of  $n^2 - k^2$  versus  $\lambda^2$  in the free carrier absorption range by extrapolating back to zero wavelength.

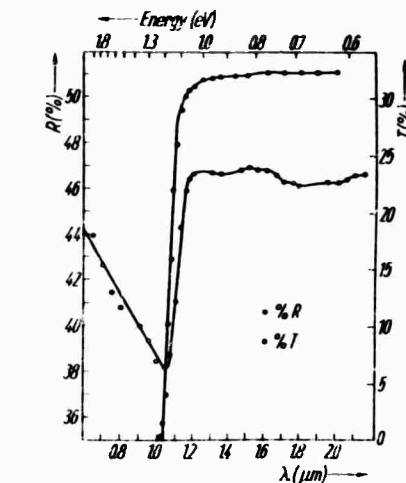
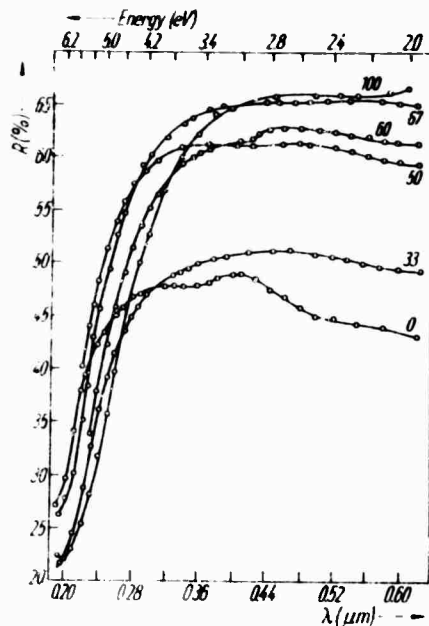


Fig. 3. The reflectance and transmission spectrum of  $\text{Sb}_2\text{Se}_3$ .

Fig. 2. The short-wavelength reflectance spectra of  $\text{Sb}_2\text{Te}_3$ - $\text{Sb}_2\text{Se}_3$  solid solutions.

has been criticised by Brust [9] on the grounds that the assignment of all peaks to the high symmetry  $\Gamma$ -Z points is too restrictive. Furthermore, Sobolev et al. [2] found no evidence of a triplet structure in their reflectivity data on  $\text{Bi}_2\text{Te}_3$ ,  $\text{Bi}_2\text{Se}_3$  and  $\text{Sb}_2\text{Te}_3$  and concluded that the reflectivity maxima have no spin-orbit nature. The band model of Borghese and Donato [10] was also too restricted to high symmetry points to satisfactorily explain their data and they suggested that assignments to the  $A(D) \langle 100 \rangle$  points should not be excluded if the triplet interpretation is omitted. It appears further calculations are needed to unravel the band structure of this class of materials.

The reflectance data for  $\text{Sb}_2\text{Se}_3$  is shown in Fig. 3. The pronounced minimum in the curve is associated with the closest approach of the valence and conduction bands and corresponds to a direct transition.

#### 4. Absorption

Transmission measurements were obtained only on those compositions containing the higher concentrations of  $\text{Sb}_2\text{Se}_3$  and are shown in Fig. 4. For the high  $\text{Sb}_2\text{Te}_3$  concentrations, no measurable transmission was obtained even for samples less than  $10 \mu\text{m}$  thick.

The absorption coefficient ( $\alpha$ ) and hence the extinction coefficient ( $k = \alpha \lambda / 4\pi$ ) was calculated from the ratio of transmitted ( $I$ ) to incident intensity ( $I_0$ )

$$\frac{I}{I_0} = \frac{(1 - R)^2 e^{-\alpha x}}{1 - R^2 e^{-2\alpha x}} \quad (2)$$

where  $x$  is the sample thickness, assuming no multiple interference effects. Calculations showed this equation to be valid even for those cases where inter-

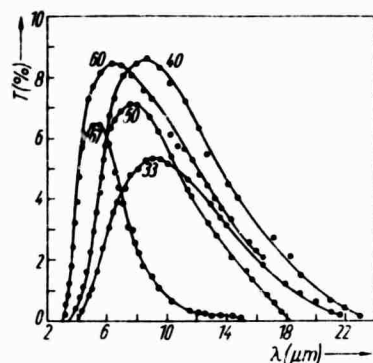


Fig. 4. The transmission spectrum of  $\text{Sb}_2\text{Te}_3\text{-Sb}_2\text{Se}_3$  solid solutions

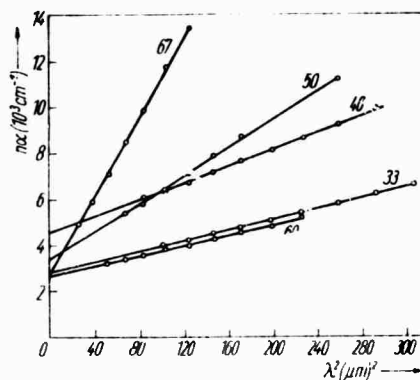


Fig. 5. The variation of the product of absorption coefficient ( $\alpha$ ) and refractive index ( $n$ ) in the free carrier absorption region with the square of the wavelength in  $\text{Sb}_2\text{Te}_3\text{-Sb}_2\text{Se}_3$  solid solutions

ference fringes were observed, leading to errors in  $\alpha$  of less than 2% for these samples. Having obtained  $k$ , the refractive index ( $n$ ) was then determined from

$$n = \frac{1 + R}{1 - R} + \sqrt{\frac{4R}{(1 - R)^2} - k^2}. \quad (3)$$

Values so obtained agreed very closely with the values of  $n$  determined from the positions of the interference fringes. The product  $n\alpha$  in the free carrier absorption range is plotted against  $\lambda^2$  in Fig. 5 and is shown to obey the relation [7]

$$n\alpha = \frac{\lambda^2 e^3 p}{4\pi^2 c^3 \epsilon_0 m_p^2 \mu_p}. \quad (4)$$

The square root of the absorption coefficient was plotted against energy (Fig. 6) for each composition and found to yield two straight lines conforming to the equation [11]

$$\alpha = A \left[ \frac{(h\nu - E_g - k\theta)^2}{1 - \exp\left(-\frac{\theta}{T}\right)} + \frac{(h\nu - E_g + k\theta)^2}{\exp\left(\frac{\theta}{T}\right) - 1} \right] \quad (5)$$

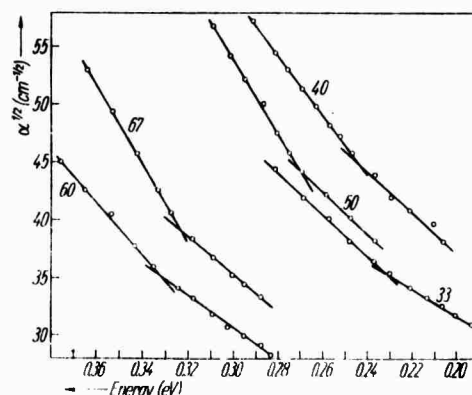


Fig. 6. Square root of the absorption coefficient versus incident photon energy

for the simplest case of indirect allowed transitions, where  $k\theta$  is the single phonon energy required to conserve momentum. By analogy with  $\text{Bi}_2\text{Te}_3$  [1] these indirect transitions should occur somewhere along the  $\Gamma A$  or  $\Gamma D$  directions of the Brillouin zone. As is generally the case for  $M_0$  type critical points no structure in the room-temperature reflectivity curves corresponding to these indirect transitions was observed [12].

An arbitrary selection of an absorption coefficient value for the absorption edge [1] did not show any regular trend in energy gap with composition. Values of the energy gap ( $E_g$ ) and  $k\theta$  determined from the intercepts of the curves with the abscissa in Fig. 6 are listed in Table 1. The  $E_g$ -values show a decreasing trend with increasing  $\text{Sb}_2\text{Se}_3$  content.

The exact values of these energy gaps are uncertain because of the indication of considerable charge carrier degeneracy from Fermi-level positions determined by Seebeck coefficient measurements. The possibility of the  $\text{Sb}_2\text{Te}_3$ - $\text{Sb}_2\text{Se}_3$  solid solutions having light and heavy hole valence bands as in  $\text{Sb}_2\text{Te}_3$  [13, 14], or that both electrons and holes are contributing to the Seebeck coefficient in these low band gap materials, does not allow an accurate designation to be made of the position of the Fermi-level from Seebeck coefficient measurements. Moreover, corrections for degeneracy, as carried out by Sehr and Testardi [15] or by Greenaway and Harbeke [1], did not allow for the fact that optical transitions may take place from levels approximately  $4kT$  (equivalent to 0.1 eV at room-temperature) away from the Fermi-level [16], i.e. at an energy spread greater than the correction applied. Therefore, no reliable estimate of the Burstein shift [16] can be made.

For pure  $\text{Sb}_2\text{Se}_3$  the energy gap occurs at about 1 eV and in contrast to the statement of Shuflov et al. [3], appears to arise from a direct allowed transition [17]. Excellent correspondence is seen in Fig. 3 between the reflectivity minimum and the point of maximum slope of the absorption edge [7].

Table 1

Sample No.	Nominal % $\text{Sb}_2\text{Te}_3$	Resistivity ( $\Omega\text{cm}$ ) (300 °K)	Seebeck coeff. ( $\mu\text{V}/\text{deg}$ ) (300 °K)	Fermi level ** (eV)	$E_g$ (eV)	$\theta$ (°K)	$\lambda_{\text{min}}$ ( $\mu\text{m}$ )
1	100	$2.18 \times 10^{-4}$	$90 \pm 2$	0.07	0.21 *)	400 to 1600 *)	8.5
2	90	$4.18 \times 10^{-4}$	$45 \pm 3$	0.14	—	—	10
3	78	—	$75 \pm 3$	0.09	—	—	11
4	67	$4.27 \times 10^{-4}$	$43 \pm 4$	0.17	0.16	775	13
5	60	$4.83 \times 10^{-4}$	$48 \pm 3$	0.14	0.14	660	15
6	50	$5.66 \times 10^{-4}$	$97 \pm 2$	0.06	0.09	660	19
7	40	$8.00 \times 10^{-4}$	$61 \pm 4$	0.11	0.04	520	23
8	33	$11.28 \times 10^{-4}$	$66 \pm 2$	0.10	0	500	24

\*) Values obtained from [15].

\*\*) Fermi level values calculated from the Seebeck coefficient assuming a one-carrier single valence band model.

### 5. Discussion

In view of the fact that  $\text{Sb}_2\text{Te}_3$  is isostructural with  $\text{Bi}_2\text{Te}_3$  and  $\text{Bi}_2\text{Se}_3$ , the highest valence band and lowest conduction band would be expected to consist of six ellipsoidal isoelectronic surfaces [2] and the Brillouin zone would be ex-

pected to exhibit the same symmetry as  $\text{Bi}_2\text{Te}_3$  [1]. The similarity in optical properties is therefore not surprising.  $\text{Sb}_2\text{Se}_3$  differs from  $\text{Sb}_2\text{Te}_3$  in its crystal structure. Thus, some differences in optical properties would be expected and are found, e.g. the smallest energy gap in  $\text{Sb}_2\text{Se}_3$  is a direct one, and splitting of several  $\text{Sb}_2\text{Se}_3$  reflectivity peaks ( $A_{4.5}$ ) occur due to lower crystal symmetry [3].

Drabble and Goodman [18] have proposed a layer structure for the  $\text{Bi}_2\text{Te}_3$  class of compounds, each layer consisting of similar atoms stacked in a sequence  $\text{Te}^{(1)}\text{-Bi-Te}^{(2)}\text{-Bi-Te}^{(1)}$  perpendicular to the three-fold axis. The superscripts denote differently bonded tellurium atoms: the  $\text{Te}^{(2)}$  atoms being surrounded almost octahedrally by covalently bonded Bi atoms, with a weak ionic component; the  $\text{Te}^{(1)}$  atoms have three nearest neighbor covalently bonded Bi atoms, with a strong ionic component, and three van der Waal bonded  $\text{Te}^{(1)}$  atoms in the adjacent layer. This model was used by Drabble and Goodman to explain the results of Austin and Sheard [19] on the variation of the optical energy gap of  $\text{Bi}_2\text{Te}_{3-x}\text{Se}_x$  alloys, and was used later by Greenaway and Harbeke [1] to explain their data on similar alloys. It was proposed that if tellurium is replaced by selenium then the more electronegative selenium atoms will substitute preferentially for the more weakly bound  $\text{Te}^{(2)}$  atoms. The increased bond strength will cause an increase in the energy gap. Eventually, when all  $\text{Te}^{(2)}$  sites are occupied, selenium then substitutes for  $\text{Te}^{(1)}$  atoms, attracting charge away from the  $\text{Bi-Te}^{(2)}$  bonds, thus causing the energy gap to decrease again.

It appears more likely that selenium is substituting for the  $\text{Te}^{(1)}$  atoms in the  $\text{Sb}_2\text{Te}_3$ - $\text{Sb}_2\text{Se}_3$  alloys. The general trend of decreasing band gaps and the transition from hexagonal to mixed phase at the composition  $\text{Sb}_2\text{Te}_3\text{Se}_2$  lend support to this view. The high hole concentration always observed in  $\text{Sb}_2\text{Te}_3$  is thought to be due to a wrong-atom defect [20] with a stoichiometric excess of Sb (providing acceptor states) on Te sites. Although it is probable, in view of the above model, that Te vacancies would occur preferentially on  $\text{Te}^{(2)}$  sites it does not necessarily follow, as Teramoto and Takayanagi [4] supposed, that it is energetically favorable for excess Sb to occupy the  $\text{Te}^{(2)}$  sites rather than the  $\text{Te}^{(1)}$  sites.

It appears that more definitive X-ray studies are required to resolve these problems.

#### References

- [1] D. L. GREENAWAY and G. HARBEKE, *J. Phys. Chem. Solids* **26**, 1585 (1965).
- [2] V. V. SOBOLEV, S. D. SHUTOV, YU. V. POROV, and S. N. SHESTATSKII, *phys. stat. sol.* **30**, 349 (1968).
- [3] S. D. SHUTOV, V. V. SOBOLEV, YU. V. POROV, and S. N. SHESTATSKII, *phys. stat. sol.* **31**, K23 (1969).
- [4] I. TERAMOTO and S. TAKAYANAGI, *J. Phys. Chem. Solids* **10**, 121 (1961).
- [5] W. PROCARIONE and C. WOOD, to be published.
- [6] J. STRONG, *Procedures in Experimental Physics*, Prentice-Hall, Inc., Englewood Cliffs (N.J.) 1938 (p. 376).
- [7] T. S. MOSE, *Optical Properties of Semiconductors*, Butterworths, London 1961.
- [8] L. R. TESTARDI, J. BIERLY, and F. DONAHUE, *J. Phys. Chem. Solids* **23**, 1209 (1962).
- [9] D. BRUST, *Phys. Rev.* **134**, 1337 (1964).
- [10] F. BORGHESE and E. DONATO, *Nuovo Cimento* **53B**, 283 (1968).
- [11] G. G. MACFARLANE and V. ROBERTS, *Phys. Rev.* **97**, 1714 (1955).

- [12] D. L. GREENAWAY and G. HARBKE, Optical Properties and Band Structure, Pergamon Press, London 1968 (p. 41).
- [13] B. RÖNNLUND, O. BECKMAN, and H. LEVY, J. Phys. Chem. Solids **26**, 1281 (1965).
- [14] I. A. SMIRNOV, A. A. ANDREEVA, and V. A. KUTASOV, Soviet Phys. — Solid State **10**, 1403 (1968).
- [15] R. SEHR and L. R. TESTARDI, J. Phys. Chem. Solids **23**, 1219 (1962).
- [16] E. BURSTEIN, Phys. Rev. **93**, 632 (1954).
- [17] Z. HURYCH and C. WOOD, to be published.
- [18] J. R. DRABBLE and C. H. GOODMAN, J. Phys. Chem. Solids **5**, 142 (1958).
- [19] I. G. AUSTIN and A. SHEARD, J. Electronics and Control **3**, 236 (1957).
- [20] T. C. HARMAN, B. PARIS, S. E. MILLER, and H. L. GOERING, J. Phys. Chem. Solids **2**, 181 (1957).

(Received August 6, 1970)

# THERMALLY MODULATED PLASMA FREQUENCY OF FREE HOLES IN THE $\text{Sb}_2\text{Te}_{3-x}\text{Se}_x$ COMPOUNDS\*

Z. Hurych and C. Wood,

Physics Department, Northern Illinois University, DeKalb, Illinois 60115

(Received 3 November 1970 by R.H. Silsbee)

The plasma resonance frequency  $\omega_p$  of free holes in a single-crystal of the narrow-band semiconductor  $\text{Sb}_2\text{Te}_{3-x}\text{Se}_x$  was obtained using thermally-modulated reflectivity. This method gave accurate values of  $\omega_p$  even in the case of broadening due to strong free-carrier and interband absorption.

SINGLE crystal solid solutions of rhombohedral  $\text{Sb}_2\text{Te}_3$  and orthorhombic  $\text{Sb}_2\text{Se}_3$  can be prepared of composition  $\text{Sb}_2\text{Te}_{3-x}\text{Se}_x$  for values of  $x$  in the range 0-2.<sup>1</sup> All of these compounds possess similar physical properties: rhombohedral ( $C_{3v}D_{3d}$ ) crystal structure;  $p$ -type conductivity with values of  $10^{-4}$ - $10^{-3}$  ( $\Omega\text{cm}$ )<sup>-1</sup>, decreasing with  $x$ ; similar reflectivity spectra with two sharp reflectivity windows, one in the u.v. region at  $\lambda \sim 2,800 \text{ \AA}$  for all samples, and the other in the i.r. region at  $\lambda \sim 9.5 \mu$  for  $\text{Sb}_2\text{Te}_3$  and at longer wavelengths with increasing  $x$ .

The long wavelength edges of these i.r. reflectivity windows were associated with the plasma resonance frequency  $\omega_p$  of free holes in the valence band. For  $\text{Sb}_2\text{Te}_3$  this assignment of a plasma window was confirmed<sup>1</sup> from the position of the minimum reflectivity. However, absorptive processes produce a broadening of the resonance pattern as well as a non-zero reflectivity at the minimum, thus complicating the exact determination of  $\omega_p$  from the reflectance spectrum. The rather

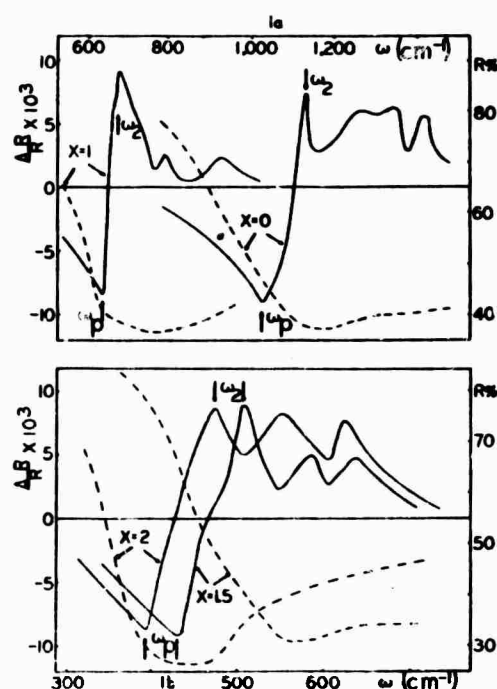


FIG. 1a, b: The reflectivity  $R$  (dashed curve) and modulated reflectivity  $\Delta R/R$  (solid curve) in the vicinity of the plasma resonance frequency for various compositions of  $\text{Sb}_2\text{Te}_{3-x}\text{Se}_x$ .

\* This research was supported by the Advanced Research Projects Agency of the Department of Defense and was monitored by the Army Research Office Durham, under Contract No. DA-ARO-D-31-124-70-G77.



Table 1.

	Sb <sub>2</sub> Te <sub>3</sub>	Sb <sub>2</sub> Te <sub>2</sub> Se	Sb <sub>2</sub> Te <sub>1.5</sub> Se <sub>1.5</sub>	Sb <sub>2</sub> TeSe <sub>2</sub>
$\omega_p$ [cm <sup>-1</sup> ]				
from thermal modulation	1,040	645	435	393
$\omega_2$ [cm <sup>-1</sup> ]				
from thermal modulation	1,125	665	505	470
$\epsilon_L$	7.3	16.7	4.0	3.70
$\epsilon_C$				
from extrapolation $\lambda = 0$	50 *	28	42	39
$\eta$	0.410	0.158	0.860	0.925
$\omega_\tau$ [cm <sup>-1</sup> ]				
from $\eta$	426	102	375	370
$\omega_p$ [cm <sup>-1</sup> ]				
from extrapolation $\epsilon_r = 0$	1,025 *	530	490	373

\* Data from reference 7.

high concentration of free carriers ( $p \sim 10^{18} - 10^{19} \text{ cm}^{-3}$ ) affects not only the real part of the dielectric constant  $\epsilon_r$  but also the imaginary part  $\epsilon_i$  through the free-carrier absorption. Moreover, in the case of *p*-type materials, an additional contribution to  $\epsilon_r$  and to  $\epsilon_i$  due to interband transition between light and heavy hole bands generally exists,<sup>2,3</sup> which may be enhanced in the case of spin-orbit splitting of the valence bands. Therefore, thermomodulated reflectivity experiments were performed on the Sb<sub>2</sub>Te<sub>3-x</sub>Se<sub>x</sub> compounds in order to obtain accurate values of  $\omega_p$  and to confirm the plasma oscillation assignment.

All samples could be cleaved easily along natural cleavage planes (0001) thus allowing the preparation of thin single crystal specimens, 20–50  $\mu$  thick. With this sample orientation the electric vector *E* of the incident radiation was perpendicular to *c*-axis throughout our measurements. Square-wave current pulses with peak values of from 500 mA up to 2.0 A at a frequency of 11 c/s were passed through the samples. A modified Beckmann i.r.-12 Spectrophotometer was used, such that the modulated 11 cps signal from the thermopile detector was fed to a Keithley 802 Series Lock-in Amplifier and then recorded.

The thermoreflectance spectra of the samples are shown in Fig. 1 together with the reflectance spectra. All of the samples exhibit the typical feature: of a thermally modulated plasma frequency,

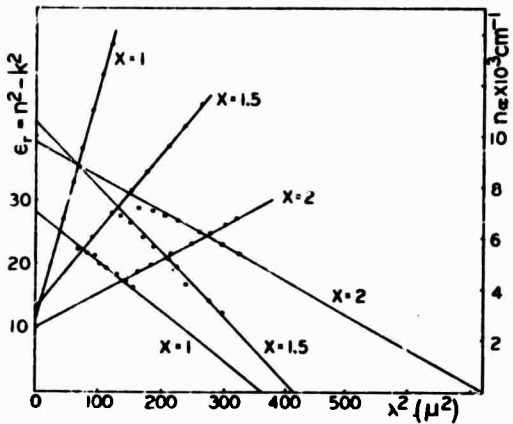


FIG. 2. The real part of the dielectric constant,  $\epsilon_r = n^2 - k^2$  and the free-carrier absorption ( $n \cdot \alpha$ ) versus the square of the wavelength ( $\lambda^2$ ) for the Sb<sub>2</sub>Te<sub>3-x</sub>Se<sub>x</sub> compounds.

i.e. two sharp peaks of opposite sign.<sup>4</sup> One of the peaks ( $\omega_p$ ) corresponds to the thermal modulation of the plasma frequency  $\omega_p$  (in these narrow gap semi semiconductors,  $\omega_p$  is modulated both by change of carrier concentration, *p*, as well as by change of the effective mass  $m_e^*$ ), and the other peak ( $\omega_2$ ) corresponds to the modulation of the broadening parameter  $\eta = \omega_\tau / \omega_p$ , (where  $\omega_\tau$  is the collision frequency which express phenomenologically the scattering of free carriers by phonons). The shorter wavelength side of the thermomodulated spectra shows additional structure which may be

due to transitions between the light and heavy hole bands.<sup>2,3</sup> Light and heavy hole bands have been postulated to explain thermoelectric<sup>5</sup> and Hall effect data<sup>6</sup> in this class of compounds and appear to indicate a heavy to light hole concentration of at least two orders of magnitude. This large concentration ratio, even allowing for the lower effective mass of light holes, would suggest that a plasma resonance frequency due to the light holes would occur somewhere in the far i.r. region of the spectrum [see equation (2)], and that heavy holes are responsible for the plasma resonance observed.

From the two frequencies  $\omega_p$  and  $\omega_2$ , the non-dispersive dielectric constant of the lattice  $\epsilon_L$  and the broadening parameter  $\eta$  can be determined using the relations<sup>4</sup>

$$\epsilon_L \left[ 1 - \left( \frac{\omega_p}{\omega_2} \right)^2 \right]^{-1} \text{ and } R(\omega_2) \left[ \frac{\epsilon_L \omega_p^3 \eta}{4 \omega_2^2} \right]^2. \quad (1)$$

These results are shown in Table 1 together with calculated values of  $\omega_p$  and of the optical dielectric constant  $\epsilon_C$ ; the latter was determined from the extrapolation of the spectral dependence of  $n^2 - k^2$  in the free carrier absorption range to  $\lambda = 0$ . (Fig. 2;  $n$  and  $k$  were obtained from transmission and reflectivity measurements.<sup>1</sup>)

Extrapolation of the same curves to  $n^2 - k^2 = 0$  gave values of  $\omega_p'$  in reasonable agreement with the values of  $\omega_p$  obtained from thermal modulation while values of  $\epsilon_L$ , determined from equation (1) were quite different from  $\epsilon_C$ , which is obviously

due to large discrepancy between the wavelength at which minimum reflectivity occurs and the wavelength where  $\epsilon_r = n^2 - k^2 = 1$  [ $\epsilon_L$  has very strong dependence on  $(\omega_p/\omega_2)$ ]. A similar discrepancy can be found in case of Sb<sub>2</sub>Te.<sup>7</sup> This discrepancy can be due either to interband transitions between light and heavy hole bands which contribute to the real,  $\epsilon_r$ , and imaginary,  $\epsilon_i$ , parts of the dielectric constant, similar to the case of *p*-type germanium,<sup>3</sup> or to a high collision frequency  $\omega_2$  such that the condition  $(\omega_p/\omega_r)^2 \gg 1$  is not valid. For either case, the expression:

$$\epsilon = \epsilon_C - \frac{4\pi p}{m_C^* \omega (\omega + i \omega_r)} \quad (2)$$

for the total dielectric constant does not apply, so equation (1) cannot be used without modification.

Existence of either of the above phenomena is supported by an absorption background resulting in high values of the free carrier absorption background resulting in high values of the free carrier absorption ( $\sim 10^3 \text{ cm}^{-1}$ ) as extrapolated to  $\lambda = 0$ . However, the additional structure in the thermomodulated spectra as well as the calculation of  $\omega_p$  from the Hall mobility data<sup>7</sup> indicate that the effect of interband transitions is more probable. These transitions are therefore also responsible for the discrepancy between  $\omega_p$  and  $\omega_p'$ .

The advantage of thermomodulating the reflection spectra is clearly indicated by the fact that despite very strong broadening due to competing absorption processes,  $\omega_p$  can be determined with high accuracy.

#### REFERENCES

1. PROCARIONE W. and WOOD C., to be published in *Phys. Status Solidi* 42, No. 2, (Dec. 1970).
2. FAN H.Y., *Semiconductors and Semimetals*, Vol. 3, p. 406, Academic Press (1967).
3. SPITZER W.G. and FAN H.Y., *Phys. Rev.* 106, 882 (1957).
4. CORDONA M., *Solid State Physics*, Suppl. 11, p. 118, Academic Press, N.Y. (1967).
5. RONNLUND R., BECKMAN O. and LEVY H., *J. Phys. Chem. Solids* 26, 1281 (1965).
6. SMIRNOV I.A., ANDREEV A.A. and KUTASOV V.A., *Sov. Phys. Sol. State* 10, 1403 (1968).
7. SEHR R. and TESTARDI L.R., *J. Phys. Chem. Solids* 23, 1219 (1962).

Die Plasmaresonanzfrequenz  $\omega_p$  von freien Löchern in Einkristallen des Schmalband-Halbleiters Sb<sub>2</sub>Te<sub>1-x</sub>Se<sub>x</sub> wurde mit Hilfe von thermisch modulierten Reflektivitätsmessungen bestimmt. Mit dieser Methode erzielt man sogar dann genaue Ergebnisse, wenn Verschmierung durch starke Absorption der freien Träger auftritt oder wenn Interbandabsorption stattfindet.